ISSN 0869-5911, Petrology, 2011, Vol. 19, No. 2, pp. 134–166. © Pleiades Publishing, Ltd., 2011.
Original Russian Text © N.V. Gorbach, M.V. Portnyagin, 2011, published in Petrologiya, 2011, Vol. 19, No. 2, pp. 140–172.

Geology and Petrology of the Lava Complex of Young Shiveluch Volcano, Kamchatka

N. V. Gorbach[a] and M. V. Portnyagin[b, c]

[a] *Institute of Volcanology and Seismology, Far East Branch, Russian Academy of Sciences, bul'v. Piipa 9, Petropavlosk-Kamchatskii, 683006 Russia*
e-mail: n_gorbach@mail.ru
[b] *Vernadsky Institute of Geochemistry and Analytical Chemistry, Russian Academy of Sciences, ul. Kosygina 19, Moscow, 119991 Russia*
[c] *Leibniz Institute of Marine Sciences (IFM-GEOMAR), Wischhofstr. 1-3, D-24148, Kiel, Germany*
e-mail: mportnyagin@ifm-geomar.de

Received April 10, 2010; in final form, July 20, 2010

Abstract—Detailed geological and petrological–geochemical study of rocks of the lava complex of Young Shiveluch volcano made it possible to evaluate the lava volumes, the relative sequence in which the volcanic edifice was formed, and the minimum age of the onset of eruptive activity. The lavas of Young Shiveluch are predominantly magnesian andesites and basaltic andesites of a mildly potassic calc–alkaline series (SiO_2 = 55.0–63.5 wt %, Mg# = 55.5–68.9). Geologic relations and data on the mineralogy and geochemistry of rocks composing the lava complex led us to conclude that the magnesian andesites of Young Shiveluch volcano are of hybrid genesis and are a mixture of silicic derivatives and a highly magnesian magma that was periodically replenished in the shallow-depth magmatic chamber. The fractional crystallization of plagioclase and hornblende at the incomplete segregation of plagioclase crystals from the fractionating magmas resulted in adakitic geochemical parameters (Sr/Y = 50–71, Y < 18 ppm) of the most evolved rock varieties. Our results explain the genesis of the rock series of Young Shiveluch volcano without invoking a model of the melting of the subducting Pacific slab at its edge.

DOI: 10.1134/S0869591111020068

INTRODUCTION

Shiveluch in the northern most active volcanic center in Kamchatka (Fig. 1a), which attracts much attention of researchers because of its certain unique features. The Holocene activity of the volcano related to the Young Shiveluch eruptive center was characterized by powerful Plinian eruptions and the growth of extrusive domes. The volume of the erupted products and the frequency of eruptions make this volcano the most active explosive center in Kamchatka (Ponomareva et al., 2007). Shiveluch is the second most productive volcano (after Klyuchevskoi volcano; 36 million tons per year) and has no analogues among Quaternary volcanoes in the Kurile–Kamchatka island arc in terms of the amount of erupted andesites (Melekestsev et al., 1991). Magnesian andesites erupted by this volcano is atypical of other active volcanoes in Kamchatka (Volynets, 1994). A combination of the unique geodynamic setting of the volcano (the Shiveluch volcanic massif is spatially related to the junction zone of the Kurile–Kamchatka and Aleutian arcs) and the occurrence of magnesian andesites among its erupted products gave rise to the hypothesis that this volcano is fed by melting products of the Pacific plate subducted beneath northern Kamchatka (Yogodzinski et al., 2001; Churikova et al., 2001; Münker et al., 2001).

In spite of the paramount importance attached to the Shiveluch volcanic massif in modern models for magma generation in Kamchatka, its geological structure and the petrography, mineralogy, and geochemistry of its rocks are known inadequately poorly. This makes it impossible to test in detail of alternative models for the genesis of magmas of the Shiveluch Massif, for example, such as the model of the mixing of evolved and primitive magmas in the feeding system of the volcano, which can explains the genesis of magnesian andesite without invoking melting of subducted slab (see, for example, Streck et al., 2007).

This publication presents results of our detailed studies of the petrography, mineralogy, and geochemistry of rocks of the lava complex of Young Shiveluch volcano and our detailed field study of the volcanic edifice. These data indicate that magma mixing was a widespread process during the modern evolution of the volcano, and this can explain its high activity and the occurrence of magnesian andesites among the erupted rocks. The "adakitic" geochemical characteristics of andesites at Young Shiveluch and the low Y concentrations and elevated Sr/Y ratios of the rocks

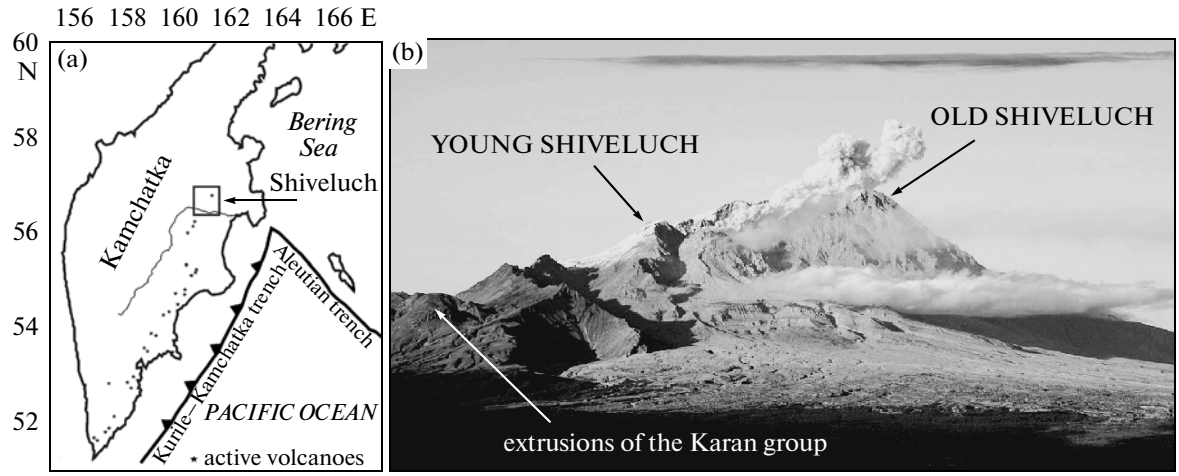

Fig. 1. Location map of the Shiveluch volcanic massif. (a) Location map; (b) volcano view from the south and its major structural features.

can be accounted for by the crystal fractionation of the parental basaltic magma with the participation of amphibole in the middle to upper crust.

MATERIALS

General Characterization of the Volcanic Edifice

The Shiveluch volcanic massif covers an area of more than 1000 km^2 in the northern part of the Central Kamchatkan Depression (Fig. 1a). Relations between the moraine of the second stage of the Late Pleistocene glaciation constrain the age of this volcano to 60–70 Ka (Melekestsev et al., 1991). The Late Pleistocene polygenetic stratovolcano of Old Shiveluch and Young Shiveluch, which was active in the Holocene (Fig. 1b), are the major structural elements of the massif (Melekestsev et al., 1991). The northern part of Old Shiveluch is a cone with steep slopes, whose summit stands 3283 m high. The southern sector of the volcanic massif was destroyed by a large–scale collapse before the onset of the second stage of the Late Pleistocene glaciation (Melekestsev et al., 1991). The eruption center of Young Shiveluch in the northwestern part of the collapse crater significantly erupted no less than 60 times in the Holocene, and these eruptions gave rise to thick pyroclastic flows, debris avalanches, ash falls, and lahars (Ponomareva et al., 2007). A series of satellite extrusion domes of the Karan group (Figs. 2, 3b), which were produced roughly simultaneously with Young Shiveluch, sit on the western slope of Old Shiveluch.

The edifice of Young Shiveluch has an area of 40 km^2 in map view and comprises extrusion domes, lava flows, and a few dikes of diverse morphology, degree of their preservation, composition, and age (Fig. 3b). The northwestern sector of the edifice is made up of the Chetvertaya Vershina extrusion. This is the topmost point of Young Shiveluch (2763 m a.s.l.). The steep western slopes consist of andesite lavas from two closely spaced extrusions, which are referred to as Cape Gorelyi (Menyailov, 1955). The eastern slopes are composed of lava flows of various composition and length. The central part of the Young Shiveluch edifice is occupied by an active crater, which was formed by the November 12, 1964, eruption and hosts a growing extrusion dome. The southern piedmont is covered with Holocene pyroclastics over an area of approximately 250 km^2.

Morphology and Structure of Young Shiveluch Volcano and Extrusions of the Karan Group

The **northeastern sector** of Young Shiveluch volcano consists of flows of *Ol–Px–Pl* ± *Hbl* andesite and *Ol–Cpx–Pl* basaltic andesite lavas. The flows originate from an elevation of approximately 2000 m and compose narrow, nearly parallel steps up to 25 m high. The thickest and longest flow was traced downward to an elevation of 1200 m. An exposure in the right-hand side of the Sukhoi Il'chinets River (Fig. 4a) shows that the flow is zonal: the top and bottom parts consist of brown brecciated lava, while the central part is made up of lava with massive subvertical joining (Fig. 4b), which locally gives way to thin platy parting along the lava flow. The thickness of the flow is 40–50 m, and its length is 4 km.

In the northeastern slope of Young Shiveluch volcano, we found extrusive bodies that have not been previously documented in the literature. These are extrusions of relatively small volume in the marginal part of the glacier saddle between the Main Summit of Old Shiveluch volcano and the edifice of Young Shiveluch, which we referred to as Ledovaya and Razrushennaya, respectively (Figs. 4c, 4d). The Ledovaya extrusion (56.64232 N, 161.33478 E, elevation 2370 m) has a flat summit and smoothed slopes (Fig. 4c), is elongated to

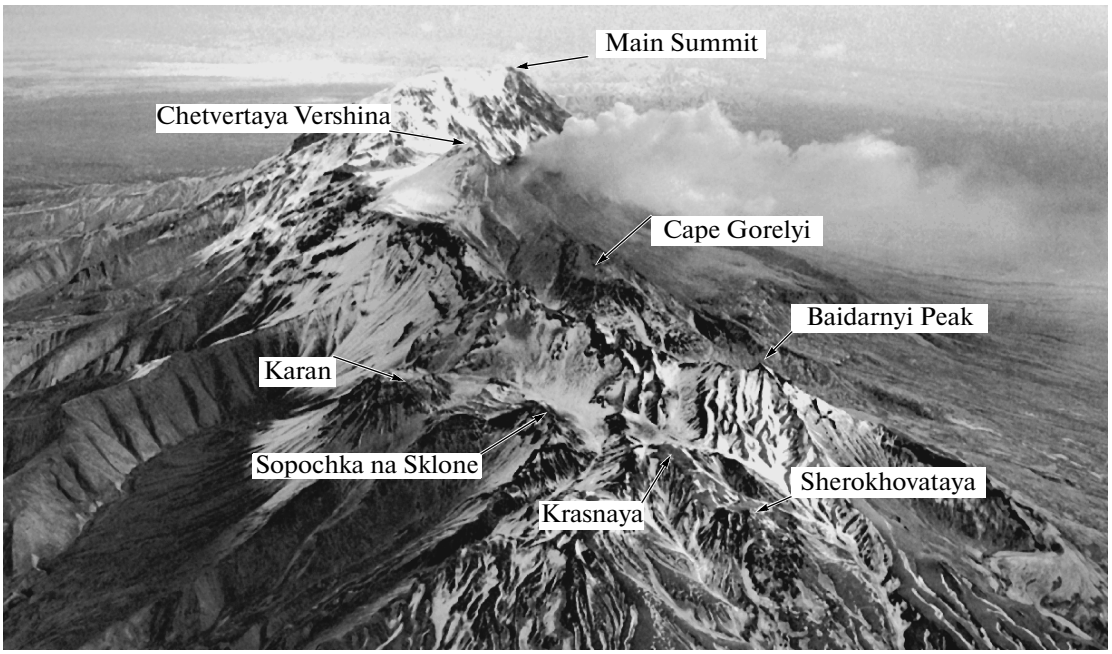

Fig. 2. View of Young Shiveluch volcano from the southwest. The figure shows major geographic names mentioned in the text. Photo: A.V. Sokorenko.

the northwest, and is exposed for a height of approximately 200 m above the modern glacier. The lavas of this extrusion display spheroidal parting, which spheres 20–30 cm across. The cores of the spheres consist of fully crystalline gray rock, and their peripheries have brown oxidized rims 2–3 cm thick. The morphology of the extrusions and the chilled structure of the lavas led us to class them with the tuya type of subglacial eruptions.

The Razrushennaya extrusion (56.64055 N, 161.33778 E, elevation 2150 m) is located between the Il'chinets Glacier and its small right-hand tributary (Fig. 4d). The narrow icefall between the tributary and main glacier body actively erodes the eastern slope of the extrusion. The northern slope is not as steep and contains a small block-lava flow in its bottom portion. A northwest-trending dike 100 m down the slope is up to 7 m thick and trends for 150 m.

Lava flow suite of the southeastern sector. The southeastern wall of the modern crater exposes a number of thinner and shorter lava flows. The origin of these flows is obliterated by an arc-shaped ledge of the older crater, which runs at a distance of approximately 400 m nearly parallel to the modern crater rim. The lower flows of brownish basaltic andesite lavas are 3–3.2 km long and 20–25 m thick and are overlain by shorter flows of andesite and heterotaxitic lavas. The most interesting flow is composed of heterotaxitic lava (Fig. 4e). The lavas exhibit bands, lenses, and embayments of broadly variable size: from a few dozen centimeters to microscopic segregations of *Hbl–Pl* andesite in brown *Ol–Cpx–Pl* andesite.

The **western and central parts** of Young Shiveluch volcano consist of *Hbl–Pl* lavas. The largest extrusion is the Chetvertaya Vershina, which looks like (when viewed from the west) as a geometric cone with steep (40°–45°) slopes smoothened by a thick cover of pyroclastic material (Fig. 2). The geometric character of the slopes is disturbed only at the very top by single lava obelisks. The piedmonts of the fragments of two closely spaced 650–700 m high Cape Gorelyi extrusions south of the Chetvertaya Vershina occur at an elevation of 1450 m. The eastern slopes of the Chetvertaya vershina and Cape Gorelyi cut off the wall of the modern crater that was produced by the 1964 eruption. The morphology of the crater is described in (Gorshkov and Dubik, 1969; Dvigailo, 1984). The crater is elongated sublatitudinally, with its greatest size in this direction reaching 1750 m. The walls at Chetvertaya Vershina are as high as 580 m, and their height decreases to 360 m in the northern part of the crater. The southeastern walls of the crater had a height of 150–170 m before the current eruption and exposed flows of heterotaxitic and basalt andesite lavas. During the current eruption (which started in December 2006 and still continues), the southeastern sector of the crater was filled with rudaceous ash flows (glowing avalanche).

Now the crater is filled with lavas of the modern extrusion dome and its debris mantle (Zharinov and Demyanchuk, 2008). The growing dome (Fig. 4e) is a morphologically complicated extrusion. The emplacement of viscous andesite lava during its early growth in 1980–1981 and in 1993–1995 formed an extrusion dome

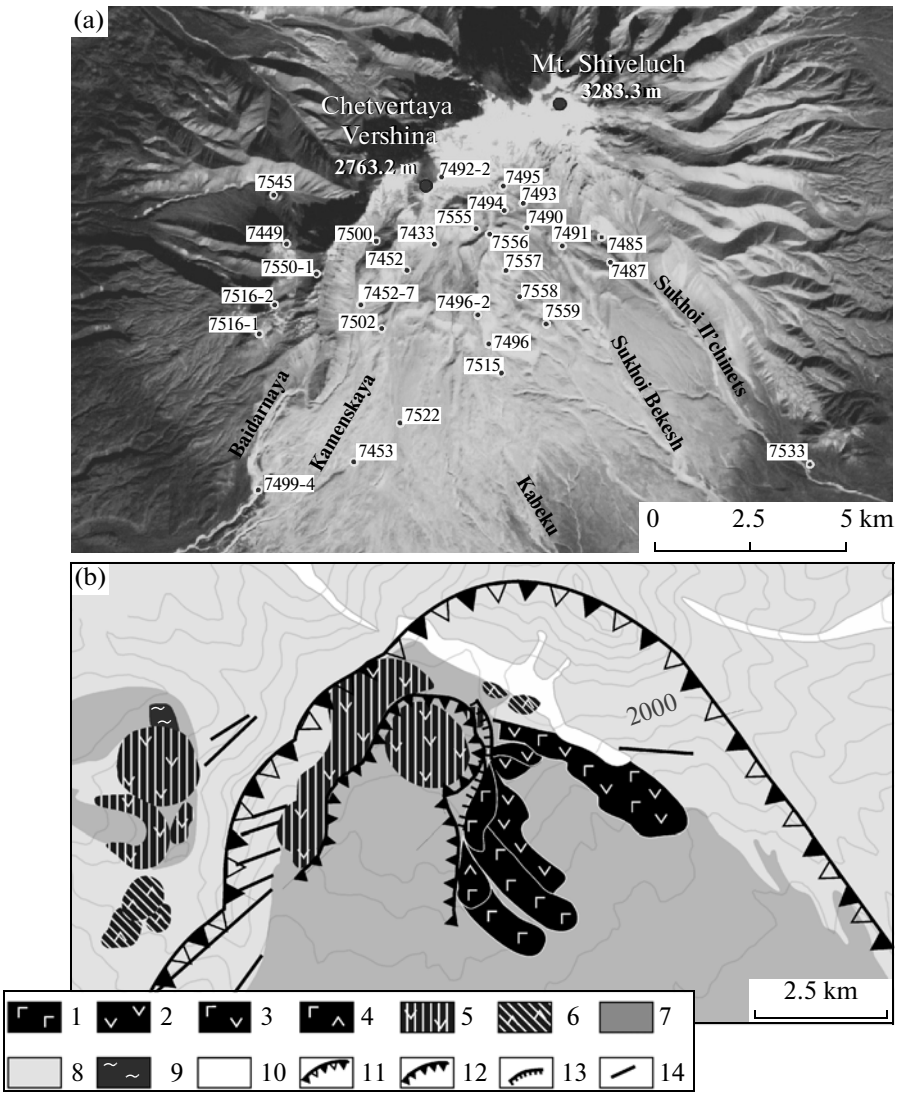

Fig. 3. Geological structure and setting of the examined rock samples of the lava complex of Young Shiveluch volcano. (a) Sampling sites of lavas of Young Shiveluch. (b) Schematic geological map of the lava complex of Young Shiveluch and extrusions of the Karan group. Lava flows: (1) *Ol–Cpx–Pl* basaltic andesite, (2) *Hbl–Px–Pl* andesite, (3) *Ol–Px–Pl* ± *Hbl* basaltic andesite, (4) heterotaxitic lavas. Extrusive lavas: (5) *Hbl–Pl* and *Hbl–Px–Pl* andesite, (6) *Ol–Hbl* ± *Pl* and *Ol–Px–Pl* ± *Hbl* andesite. Other symbols: (7) proximal pyroclastic deposits and debris avalanche deposits of Young Shiveluch volcano, (8) lavas and pyroclastic deposits of Old Shiveluch volcano, (9) block of sedimentary rocks, (10) modern glaciers, (11) crest of the Late Pleistocene collapse crater, (12) modern crater, (13) fragments of older craters of Young Shiveluch, (14) dikes.

that shows all typical structural and morphological features (Dvigalo, 1984; Khubunaya et al., 1995; Melekestsev et al., 2004). The 2001–2009 explosive–extrusive eruptions dynamically modified the dome morphology. The 2001–2002 explosive lava eruptions occurred at various sites within the crater (Fedotov et al., 2001). The squeezing of rigid lava blocks at the cone summit in 2004 gave way to eruptions of a block-lava flow onto its southeastern slope (Gorbach, 2006). A new large extrusive block was produced in the western part of the crater in 2005. The current eruption (that started in December 2006 and continues until nowadays) has a high supply rate of extrusive lavas to the eastern and central sectors of the dome.

Extrusions of the Karan group. Nearly synchronously with the development of Young Shiveluch volcano, a number of extrusions were formed (extrusions of mounts Karan, Sopochka na Sklone, Krasnaya, and Sherokhovataya) at approximately 5 km west of it (Fig. 2)[1]. Menyailov (1955) believed that the extrusions were

[1] The names Karan and Sopochka na Sklone are sometimes used ambiguously in the topographic maps and literature; we adhere herein to the usage of the name Karan with reference to the northernmost extrusion with an elevation of 1823.3 m, as is shown in the 1 : 50000 topographic map.

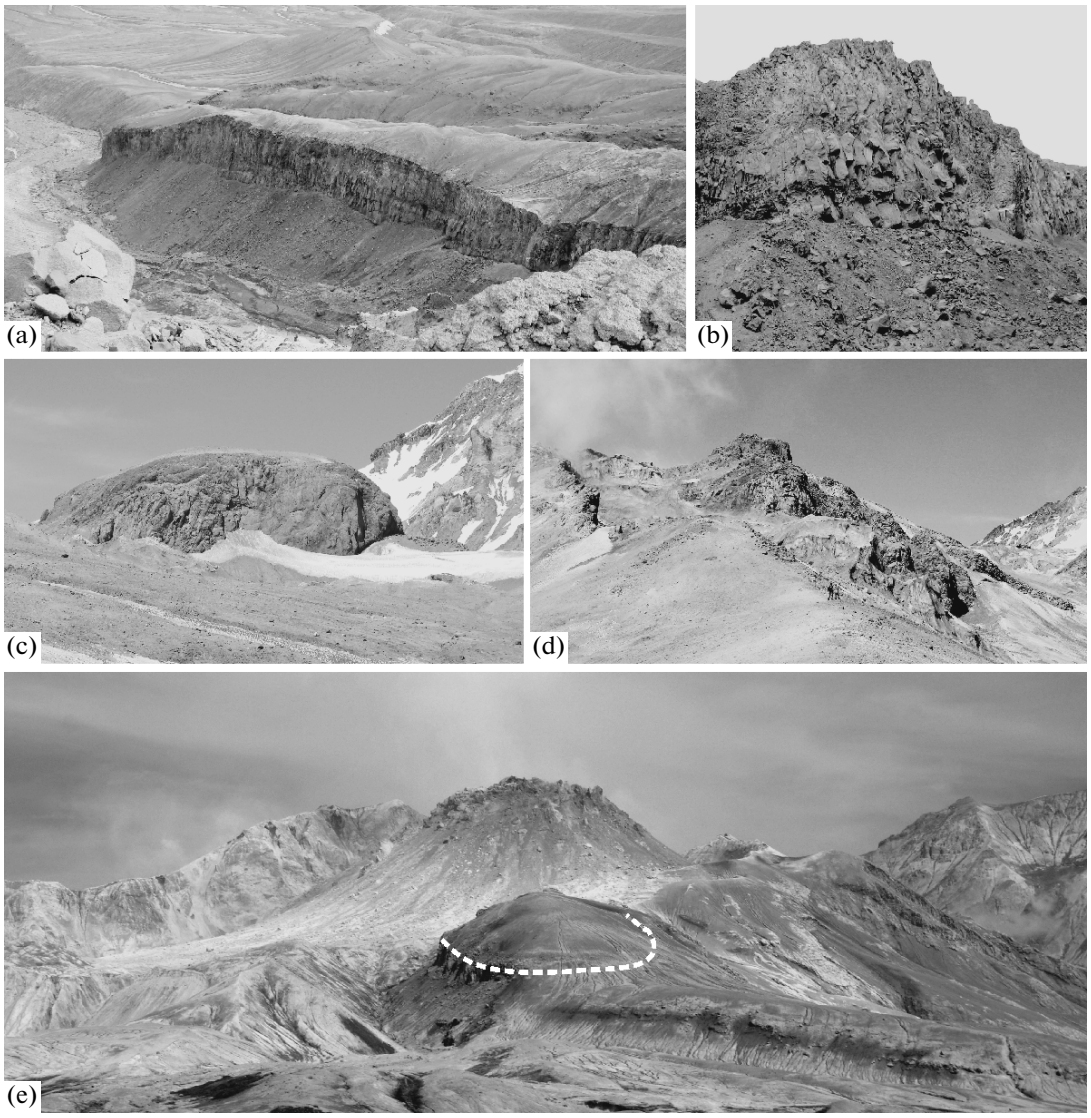

Fig. 4. Lava in the eastern sector of Young Shiveluch volcano. (a) Longest lava flow on the eastern slope; (b) lava parting in the flow; (c) Ledovaya extrusion; (d) Razrushennaya extrusion; (e) southeastern sector of Young Shiveluch, the dashed line contours a flow of heterotaxitic lavas with an active extrusive dome above its (at the center of the figure).

emplaced in relation to the northeast-trending fault that cuts the western slopes of the Late Pleistocene edifice of Old Shiveluch.

The extrusion of Mount Karan is a dome of complicated structure, 2 km in diameter at the basement, which was formed by multiple emplacements of *Hbl–Px–Pl* andesite. At the northern margin of the dome, the extrusion hosts a block of sedimentary rock of supposedly Neogene age (Lopatin et al., 1979). The southern part of Mount Karan is adjacent to an extrusive body (which is referred to as Mount Sopochka na Sklone), whose western sector is demolished and faces the valley of the Karina River. According to (Ponomareva et al., 2007), the pyroclastic flows and debris avalanches related to the activity of these extrusions have an age of 1900 and 1450 ^{14}C years, respectively. The extrusions are separated by a small thermal area (Menyailov, 1955) with numerous low-discharge and low-temperature fumarole jets.

The extrusions of mounts Sherokhovataya and Krasnaya 1 km south of Mount Karan are two adjacent domes approximately 1.5 km in diameter at the basement and relative heights of 150–200 m. Judging from their morphological features, these extrusions are older than mounts Karan and Sopochka na Sklone. The lavas of mounts Sherokhovataya and Krasnaya differ in composition from those of more northerly extrusions and are *Ol–Hbl* ± *Pl* andesites.

Age and Development Sequence of the Young Shiveluch Volcanic Edifice

Field relations led us to believe that the activity of Young Shiveluch volcano started in the vicinity of the glacier saddle with the emplacement of extrusions and eruptions of olivine–pyroxene–plagioclase amphibole-bearing andesite and basaltic andesite lavas (Ledovaya and Razrushennaya extrusions and lava flows originating from the northeastern part of the edifice). The Ledovaya and Razhrushennaya extrusive bodies show evidence of their interaction with the glacier, and this suggests that the extrusions could be produced during the Late Pleistocene glaciation. Debris avalanche deposits exposed in the left-hand wall of the valley of the Sukhoi Il'chinets River (site 7533) contain rock fragments compositionally close the lava flows and extrusions in the northeastern sector of Young Shiveluch. The lower debris avalanche unit consists of reddish gray material with fragments of *Hbl–Pl* andesite and *Ol–Cpx–Pl* basaltic andesite (Tables 1, 2: samples 7533-2 and 7533-2a). The upper unit is made up of pale gray material with fragments of *Ol–Cpx–Pl* and *Ol–Px–Pl* ± *Hbl* rocks (samples 7482, 7533-4, and 7533-5), whose petrography and chemistry are similar to those of the lavas (samples 7485-1, 7487, 7493, and 7495) in the northeastern sector of Young Shiveluch. A sample of wood taken from below the bottom of the upper debris unit yielded a radiocarbon age of 10240 ± 160 ^{14}C years (sample GIN 14077). The petrographic and petrochemical similarities of the material of the upper debris unit and the oldest lava flows and extrusions of Young Shiveluch (Tables 1, 2) suggest that the eruptive activity of the volcano started no earlier than ~10000 ^{14}C years, likely late during the second phase of the Late Pleistocene glaciation.

The sources of the flows in the southeastern sector of Young Shiveluch, including those of heterotaxitic lavas, were reconstructed as originating from the modern crater, and this testifies that the eruption center shifted to the southwest. Conceivably, the age of these compositionally heterogeneous flows can be correlated with the eruption at 3700 ^{14}C years, which predated the eruption of *Ol–Cpx–Hbl* ± *Pl* basalt at 3600 ^{14}C years. Judging by the database in (Ponomareva et al., 2007), only the tephra of this eruption has fragments of heterogeneous composition (samples 00K20A1, 00K20A2, 00K20B, 00K22, and 00K23) identical to the contrasting composition of lavas in the southeastern sector.

Extrusive bodies in the western sector of the Young Shiveluch edifice are younger. According to (Melekestsev et al., 2003), the largest extrusion of Chetvertaya Vershina is younger than approximately 1030 years and the ~1430 eruption has destroyed its southeastern sector.

Lava Volumes at Young Shiveluch Volcano

The maximum volume of lavas observable at Young Shiveluch does not exceed 25 km^3, and the lava volume of extrusions of the Karan group is approximately 3 km^3. For a volcano whose eruptive activity is characterized by the destruction of its extrusive domes and the development of debris avalanches, these estimates correspond only to the volume of the now preserved geological bodies but not to the actual volume of lavas erupted by the volcano. For example, the debris avalanche of the 1964 catastrophic eruption has destroyed five extrusive domes in the central sector of Young Shiveluch (Gorshkov and Dubik, 1969). The volume of the removed portion of the edifice is evaluated (Melekestsev et al., 2003) at 1.5–1.8 km^3. The Holocene history provides record of no less than 14 debris avalanches related to the activity of Young Shiveluch and extrusions of the Karan group (Ponomareva et al., 1998). Tking into account the debris avalanches, the volume of Young Shiveluch lavas can be close to ~50 km^3, which corresponds to one-third of the total volume of products erupted by the volcano in the Holocene (calculated based on the "production rate" of the volcano of 36 million tons per year; Melekestsev et al., 1991).

METHODS

Our fieldwork involved geochemical sampling at all extrusive bodies, lava flows, and scarce dikes composing the Young Shiveluch edifice and extrusions of the Karan group on the western slope of Old Shiveluch. Figure 3a illustrates the sampling pattern. The coordinates of the samples selected for detailed examination and their brief descriptions are presented in Table 1.

Thirty eight representative samples deemed to characterize the diversity of all Young Shiveluch lavas were selected for geochemical analyses. Major elements (Si, Ti, Al, Fe, Mn, Mg, Ca, Na, K, and P) and some trace elements (V, Cr, Co, Ni, Ga, Sr, Rb, Ba, Zr, Nb, Y, and Zn) were analyzed in rock samples by XRF (on a Phillips X Unique PW1480 spectrometer) at IFM-GEOMAR in Kiel, Germany. Rock samples were analyzed together with the internationally certified rock standards JB-2, JB-3, and JA-2.

The chemistry of rock-forming minerals was analyzed in monomineralic polished sections on a JEOL JXA-8200 microprobe equipped with five wave-dispersive microprobe spectrometers at the IFM-GEOMAR in Kiel, Germany. The analyses were made with a focused beam at an accelerating voltage of 15 kV and a beam current of 100 nA for olivine and 20 nA for plagioclase, amphibole, pyroxene, and spinel. For the sake of standardization and quality control, the standards were internationally certified mineral standards (Jarosevich et al., 1980).

The compositional variability of minerals and interstitial glasses in compositionally distinct domains

Table 1. Rock samples from the lava complex of Young Shiveluch volcano

No.	Sample	Geographical coordinates	Sampling site	Sampled material	Petrography type
1	7433	N56.63219 E161.31098	Modern extrusive dome	Extrusive lavas, 2004 eruption	*Hbl-Pl* andesite
2	7449	N56.63230 E161.24328	Karan extrusion	Extrusive lavas	*Px-Hbl-Pl* andesite
3	7452-1	N56.63199 E161.30454	Modern extrusive dome	Extrusive lavas, 2005 eruption	*Hbl-Pl* andesite
4	7452-7	N56.61212 E161.26836	Modern extrusive dome	Glowing avalanche material, 2005 eruption	*Hbl-Pl* andesite
5	7453	N56.56935 E161.24670	Upper reaches of the Kamenskaya River	Pumice from pyroclastic flow, 1964 eruption	*Hbl-Pl* andesite
6	7482	N56.56866 E161.47090	Middle reaches of the Sukhoi Il'chinets River	Debris avalanche material	*Ol-Cpx-Pl* basaltic andesite
7	7485	N56.63187 E161.38018	NE sector of the Young Shiveluch edifice	Dike	*Ol-Cpx-Pl* basaltic andesite
8	7485-1	N56.63187 E161.38018	NE sector of the Young Shiveluch edifice	Late breccia	*Hbl-Pl* andesite
9	7487	N56.62871 E161.37773	NE sector of the Young Shiveluch edifice	Lava flow	*Ol-Cpx* ± *Hbl* andesite
10	7491	N56.62391 E161.36591	NE sector of the Young Shiveluch edifice	Lava flow	*Ol-Cpx* ± *Hbl* andesite
11	7492-2	N56.64336 E161.31654	Chetvertaya Vershina extrusion	Extrusive lavas	*Hbl-Pl* andesite
12	7493	N56.63765 E161.34209	NE sector of the Young Shiveluch edifice	Dike	*Ol-Cpx* ± *Hbl* basaltic andesite
13	7494	N56.63881 E161.32789	NE sector of the Young Shiveluch edifice	Extrusive lavas	*Px-Hbl* andesite
14	7495	N56.64232 E161.33478	Ledovaya extrusion	Extrusive lavas	*Ol-Cpx* ± *Hbl* basaltic andesite
15	7496	N56.60498 E161.33498	SE sector of the Young Shiveluch edifice	Lava flow	*Ol-Cpx-Pl* basaltic andesite
16	7496a	N56.61130 E161.32859	SE sector of the Young Shiveluch edifice	Lava flow	*Ol-Cpx-Pl* basaltic andesite
17	7496-1	N56.60498 E161.33498	SE sector of the Young Shiveluch edifice	Lava flow	*Ol-Cpx-Pl* basaltic andesite
18	7496-2	N56.61130 E161.32859	SE sector of the Young Shiveluch edifice	Lava flow	*Hbl-Pl* andesite
19	7496-3	N56.60921 E161.32294	SE sector of the Young Shiveluch edifice	Lava flow	*Hbl-Pl* andesite
20	7499-4	N56.56429 E161.20049	Middle reaches of the Baidarnaya River	Melanocratic nodule in rock fragment in pyroclastic flow, February 27, 2005, eruption	*Ol-Px* + *Hbl-Pl* basaltic andesite
21	7500	N56.62518 E161.26911	Cape Gorelyi extrusion	Extrusive lavas	*Hbl-Pl* andesite
22	7502	N56.61228 E161.27193	Cape Gorelyi extrusion	Extrusive lavas	*Hbl-Pl* andesite
23	7515	N56.59372 E161.32424	Headwaters of the Kabeku River	Rudaceous material in pyroclastic flow, 2007 eruption	*Hbl-Pl* andesite
24	7515-1	N56.59372 E161.32424	Headwaters of the Kabeku River	Rudaceous material in pyroclastic flow, 2007 eruption	*Hbl-Pl* andesite
25	7516-1	N56.60860 E161.22872	Krashaya extrusion	Extrusive lavas	*Ol-Hbl* andesite
26	7516-2	N56.60860 E161.22872	Sherokhovataya extrusion	Extrusive lavas	*Ol-Hbl* andesite
27	7522	N56.58615 E161.29006	Headwaters of the Kabeku River	Rudaceous material in pyroclastic flow, 2007 eruption	*Hbl-Pl* andesite
28	7533-2	N56.56935 E161.46807	Middle reaches of the Sukhoi Il'chinets River	Debris avalanche material	*Ol-Cpx-Pl* basaltic andesite
29	7533-2a	N56.56935 E161.46807	Middle reaches of the Sukhoi Il'chinets River	Debris avalanche material	*Ol-Cpx-Pl* basaltic andesite
30	7533-4	N56.56935 E161.46807	Middle reaches of the Sukhoi Il'chinets River	Debris avalanche material	*Ol-Cpx-Pl* basaltic andesite
31	7533-5	N56.56935 E161.46807	Middle reaches of the Sukhoi Il'chinets River	Debris avalanche material	*Ol-Cpx* ± *Hbl* andesite
32	7550-1	N56.61349 E161.25161	Western crest of the caldera	Erosion remnant	*Ol-Cpx-Hbl* ± *Phl* basalt
33	7555	N56.63084 E161.32245	Modern extrusive dome	Extrusive lavas, 2008 eruption	*Hbl-Pl* andesite
34	7556	N56.62713 E161.32639	SE sector of the Young Shiveluch edifice	Lava flow	*Ol-Cpx-Pl* basaltic andesite
35	7558	N56.61766 E161.34132	SE sector of the Young Shiveluch edifice	Lava flow	*Hbl-Pl* andesite
36	7559	N56.60772 E161.35253	SE sector of the Young Shiveluch edifice	Lava flow	*Px-Hbl-Pl* andesite
37	3000-1	–	Middle reaches of the Baidarnaya River	Pumice from pyroclastic flow, 2001 eruption	*Hbl-Pl* andesite
38	K1-18B	N56.52300 E161.40600	Middle reaches of the Kabeku River	Erupted tephra dated at 3600 ^{14}C years	*Ol-Cpx Hbl* ± *Phl* basalt

Note: Sample 3000-1 was made available for us by courtesy of S.A. Khubunaya (Institute of Volcanology and Seismology, Far East Branch, Russian Academy of Sciences). Geographical coordinates are presented as decimal degrees.

Table 2. Chemical composition of rock samples from the lava complex of Young Shiveluch volcano

Component	7433	7449	7452-1	7452-7	7453	7482	7485	7485-1	7487	7491	7492-2	7493	7494	7495	7496	7496a	7496-1	7496-2	7496-3
SiO_2	62.74	56.96	62.65	61.19	61.09	56.72	56.42	59.77	57.78	58.78	61.05	56.67	61.7	56.13	56.38	56.09	56.43	61	57.91
TiO_2	0.52	0.78	0.51	0.52	0.54	0.74	0.72	0.58	0.67	0.62	0.58	0.66	0.6	0.8	0.77	0.79	0.76	0.59	0.73
Al_2O_3	16.57	15.56	16.65	16.24	16.89	15.73	16.06	16.25	15.69	15.79	16.83	15.63	16.48	15.38	15.95	16.02	16	16.1	16.01
FeO	4.44	6.75	4.45	4.79	4.99	7.30	7.06	5.73	6.68	6.16	5.27	6.52	5.40	7.05	7.25	7.46	7.14	5.33	6.79
MnO	0.09	0.13	0.09	0.1	0.1	0.14	0.13	0.12	0.13	0.12	0.1	0.13	0.11	0.14	0.14	0.15	0.14	0.11	0.14
MgO	3.45	6.04	3.49	3.67	3.7	6.04	6.48	4.44	6.79	5.72	4.08	6.32	4.17	6.92	5.82	5.87	5.53	4.29	5.49
CaO	5.51	7.34	5.64	5.76	6	8	8.02	6.35	7.34	6.75	5.95	7.23	6.02	8	8.05	8.16	7.99	5.91	7.5
Na_2O	4.88	3.77	4.84	4.57	4.6	3.65	4.03	4.28	4.04	4.07	4.71	4.02	4.59	4.02	3.76	3.77	3.77	4.51	3.88
K_2O	1.2	1.52	1.24	1.42	1.27	1.31	1.08	1.36	1.16	1.25	1.2	1.18	1.33	0.73	1.27	1.2	1.28	1.38	1.29
P_2O_5	0.15	0.2	0.16	0.18	0.17	0.22	0.19	0.18	0.19	0.18	0.06	0.2	0.15	0.23	0.22	0.25	0.22	0.18	0.21
H_2O	0.29	0.35	0.23	1.48	0.79	0.14	0.17	0.83	0.12	0.31	0.52	0.19	0.14	0.30	0.24	0.47	0.33	0.48	0.27
CO_2	0.04	0.01	0.01	0.05	0.05	0.02	0.01	0.03	0.02	0.03	0.03	0.02	0.01	0.06	0.02	0.09	0.04	0.05	0.03
Total	99.88	99.41	99.96	99.97	100.19	100.01	100.37	99.92	100.61	99.78	100.38	98.77	100.70	99.76	99.87	100.32	99.63	99.93	100.25
Co	15	31	19	20	22	24	26	21	27	27	21	24	21	35	30	27	27	21	26
Cr	110	238	118	130	123	212	198	123	307	248	152	283	137	284	194	187	187	157	186
Ni	18	60	16	18	16	28	57	18	78	59	30	63	28	54	38	36	34	39	31
V	114	198	110	120	118	208	206	147	176	163	120	167	133	200	206	201	196	130	187
Zn	56	69	52	57	62	68	72	64	68	67	62	65	65	82	74	72	69	64	70
Ga	18	16	18	19	17	18	17	18	18	18	20	19	16	17	15	17	18	18	18
Rb	24	28	24	28	24	25	19	28	23	25	20	25	27	14	28	25	27	29	26
Ba	387	608	390	440	406	351	288	411	340	364	405	331	396	287	395	374	422	423	392
Sr	569	1008	579	534	565	487	453	496	470	489	576	482	524	654	521	520	525	525	515
Y	8	18	10	12	15	19	17	14	14	12	12	14	12	25	17	18	19	12	18
Zr	92	92	93	109	100	97	84	110	86	94	95	89	102	64	91	90	94	104	91
Mg#	58.1	61.5	58.3	57.7	56.9	59.6	62.0	58.0	64.4	62.3	58.0	63.3	57.9	63.6	58.8	58.4	58.0	58.9	59.0
Sr/Y	71.1	56.0	57.9	44.5	37.7	25.6	26.6	35.4	33.6	40.8	48.0	34.4	43.7	26.2	30.6	28.9	27.6	43.8	28.6

Table 2. (Contd.)

Component	7499-4	7500	7502	7515	7515-1	7516-1	7516-2	7522	7533-2	7533-2a	7533-4	7533-5	7550-1	7555	7556	7558	7559	3000-1	K1-18B
SiO_2	56.3	58.99	60.82	63.48	61.26	60.21	59.88	60.77	59.11	55.98	55.99	57.3	51.08	60.55	55.01	59.09	58.11	61.35	50.55
TiO_2	0.59	0.63	0.58	0.48	0.55	0.6	0.61	0.57	0.69	0.73	0.73	0.73	0.81	0.52	0.68	0.6	0.67	0.54	0.84
Al_2O_3	15.46	16.22	16.5	16.49	16.61	15.66	15.71	16.44	16.33	15.5	15.34	15.87	12.77	16.43	15.37	16.39	15.95	16.48	13.49
FeO	6.30	5.88	5.15	4.28	4.94	5.61	5.69	5.13	6.32	7.41	7.27	6.84	8.31	4.58	6.84	5.34	6.00	4.59	8.13
MnO	0.11	0.12	0.1	0.09	0.1	0.12	0.12	0.11	0.13	0.15	0.15	0.14	0.16	0.1	0.12	0.11	0.13	0.09	0.16
MgO	7.82	4.65	4.22	3.32	3.99	5.38	5.54	4.15	4.52	6.39	6.55	5.55	11.82	3.65	7.62	4.1	4.2	3.58	10.33
CaO	7.49	6.62	6.22	5.38	6.12	6.34	6.46	6.2	6.75	8.17	8.25	7.49	8.39	5.84	7.57	6.27	6.44	5.76	8.64
Na_2O	3.74	4.42	4.5	4.9	4.72	4.2	4.13	4.7	4.16	3.49	3.54	3.9	2.58	4.58	3.64	4.51	4.01	4.77	2.53
K_2O	0.97	1.36	1.34	1.25	1.25	1.4	1.34	1.3	1.44	1.21	1.21	1.26	1.9	1.22	0.96	1.32	1.49	1.24	1.93
P_2O_5	0.13	0.19	0.17	0.15	0.17	0.18	0.17	0.17	0.19	0.21	0.2	0.19	0.36	0.17	0.18	0.2	0.21	0.16	0.41
H_2O	0.46	0.54	0.32	0.16	0.26	0.26	0.21	0.37	0.24	0.56	0.4	0.3	0.24	0.23	0.50	0.41	0.65	0.79	0.86
CO_2	0.05	0.07	0.02	0.00	0.01	0.02	0.03	0.05	0.04	0.02	0.01	0.02	0.03	0.01	0.00	0.01	0.03	0.02	0.15
Total	99.42	99.69	99.94	99.98	99.98	99.98	99.89	99.96	99.92	99.82	99.64	99.59	98.45	97.88	98.49	98.35	97.21	99.37	98.02
Co	35	20	18	15	21	24	28	19	23	31	31	28	42	22	35	21	25	20	37
Cr	474	155	154	114	127	265	266	146	119	241	237	167	772	109	347	115	94	108	669
Ni	110	33	27	14	22	46	48	26	21	36	30	33	212	14	110	14	16	18	148
V	178	148	133	106	127	144	146	129	175	209	187	188	226	116	185	139	171	119	229
Zn	60	62	62	54	59	59	62	66	68	70	70	69	71	51	66	59	70	60	64
Ga	17	15	19	17	18	15	17	20	17	14	16	18	16	18	17	22	20	18	13
Rb	18	28	24	26	26	28	28	25	26	23	23	24	45	24	20	28	34	24	44
Ba	296	358	432	399	385	494	434	430	432	319	308	389	475	388	266	387	388	378	405
Sr	451	537	551	567	573	488	483	551	519	470	468	513	471	576	460	605	511	557	485
Y	12	17	13	12	12	12	11	13	18	19	18	20	22	15	17	16	19	12	21
Zr	68	104	96	93	99	97	96	97	113	92	91	103	84	100	87	100	117	97	93
Mg#	68.9	58.5	59.4	58.0	59.0	63.1	63.5	59.0	56.0	60.6	61.6	59.1	71.7	58.7	66.5	57.8	55.5	58.2	69.4
Sr/Y	37.6	31.6	42.4	47.3	47.8	40.7	43.9	42.4	28.8	24.7	26.0	25.7	21.2	39.2	26.7	37.4	27.1	46.4	23.1

Note: See Table 1 for sample numbers and their geological setting.

of the heterotaxitic lavas and at contacts between melanocratic nodules and host rocks were examined in polished sections, along profiles running across the contacts, using a Camebax microprobe equipped with a Kevex EDS detector at the Institute of Volcanology and Seismology, Far East Brach, Russian Academy of Sciences (analyst T.M. Filosofova). The operating conditions were as follows: the accelerating voltage was 20 kV, and the current was 40 nA. The standards were natural silicates: sanidine for Si, Na, Al, and K; diopside for Ca and Mg; olivine for Fe; ilmenite for Ti, and rhodonite for Mn.

PETROGRAPHY OF YOUNG SHIVELUCH LAVAS

Olivine–pyroxene–plagioclase amphibole-bearing andesites and basaltic andesites compose lava flows, extrusions, and dikes in the northeastern sector of Young Shiveluch volcano. Macroscopically, these are dark gray, sometimes brownish massive porphyritic or serial porphyritic rocks. The phenocrysts (30–35%) are plagioclase (15–20%), pyroxene (7–8%), olivine (up to 7%), and hornblende (2–5%), with the latter often completely opacitized. The groundmass consists of plagioclase microlites 0.02–0.1 mm long, fine-grained pyroxene aggregates, and rare olivine grains submerged in well crystallized glass. From bottom to top, the content and preservation of hornblende phenocrysts increases, and the content of olivine phenocrysts conversely decreases.

Lava flows in the southeastern sector of Young Shiveluch are compositionally heterogeneous. The lower flows consist of **olivine–clinopyroxene–plagioclase basaltic andesites**. These rocks differ from those described above in containing more clinopyroxene phenocrysts and glomerophyric aggregates and less hornblende, which is often completely dissociated. The basalt andesites are overlain by a flow of **heterotaxitic lava**, which consists of thick bands, embayments, and minute segregations of *Hbl–Pl* andesite in brown *Ol–Cpx–Pl* basaltic andesite. The differences between the compositions of the lavas are clearly seen both macro- and microscopically. The lavas contain different minerals and display different groundmass textures. The phenocrysts of the basaltic andesite lava are clinopyroxene (8–10%), olivine (up to 5%), their aggregates, and plagioclase (approximately 5%). Segregations and embayments of gray andesite contain plagioclase phenocrysts (25–30%), which are often resorbed or have a poikilitic texture in the margins, and hornblende (7–10%), whose large crystals are extensively opacitized and smaller ones are completely replaced by ore minerals.

The extrusive lavas of Chetvertaya Vershina, Cape Gorelyi, and the modern dome are **hornblende–plagioclase andesites or, more rarely, andesidacites**. These are gray, pinkish gray, and brown rocks of variable porosity, ranging from pumice to massive varieties. The lavas are porphyritic or serial porphyritic, the groundmass texture is hyalopilitic, microlitic. The structure is banded. The phenocrysts (20–50%) are plagioclase (12–30%), brown hornblende (7–25%), and pyroxenes (2–5%). Pyroxenes occur mostly as minute phenocrysts 0.2–0.4 mm long, but the rocks also contain relatively rare short-prismatic orthopyroxene phenocrysts up to 1 mm long. Some varieties contain olivine as rare round grains surrounded reaction rims of fine-grained orthopyroxene and amphibole aggregates. The lavas erupted in 2004 contain single opacitized biotite flakes. The groundmass consists of silicic glass, plagioclase microlites, apatite needles, and minor amounts of hornblende and ore mineral.

The western satellite extrusions are composed of **pyroxene–hornblende–plagioclase andesites** (extrusions of mounts Karan and Sopochka na Sklone) and **olivine–hornblende plagioclase-bearing andesites** (extrusions of mounts Sherokhovataya and Krasnaya). The *Ol–Hbl ± Pl* andesites exhibit certain distinctive features. Their fabric is defined by the strong predominance of pargasite hornblende among phenocrysts (from 0.2–0.3 to 2–3 mm long) and the presence of olivine in the cores of rare individual phenocrysts and in their aggregates. The rocks also contain large tabular andesine megacrysts up to 7–10 mm long and cristobalite in the groundmass.

Olivine–clinopyroxene–hornblende phlogopite-bearing basalts. The rocks of this unusual composition were documented in the tephra of the eruption at 3600 ^{14}C years (Volynets et al., 1997). A small primary exposure of such rocks was found in the western slope of the caldera, north of Baidarnyi Peak. This exposure was interpreted as a relic or apophyse of a larger body that occurred in the western sector of Young Shiveluch volcano.

The *Ol–Cpx–Hbl ± Phl* basalts are pale gray massive, well recrystallized rocks with large (up to 3–5 mm) forsterite phenocrysts (10–15 vol %) and abundant fine-grained needle-shaped amphibole (15–20 vol %). The rocks also contain minor amounts of clinopyroxene phenocrysts. Phlogopite was detected as single opacitized subphenocrysts. The groundmass of the rock consists of brown glass with numerous plagioclase, pyroxene, and ore mineral microlites. The composition of the interstitial glass varies from latite to potassic rhyodacite (Volynets et al., 1997).

Melanocratic nodules. Blocks of *Hbl–Pl* andesite in the 2005 pyroclastic flow contain crystalline nodules with chilled textures; the composition of these rocks corresponds to basaltic andesite. The nodules contain large, slightly corroded magnesian olivine phenocrysts with abundant inclusions of Cr-spinel. Olivine grains are sometimes surrounded by amphibole and/or pyroxene rims. The groundmass consists of needle-shaped plagioclase and amphibole and clear transparent glass with abundant large equant pores. The contacts with the host lava are sharp, sometimes with groundmass embayments.

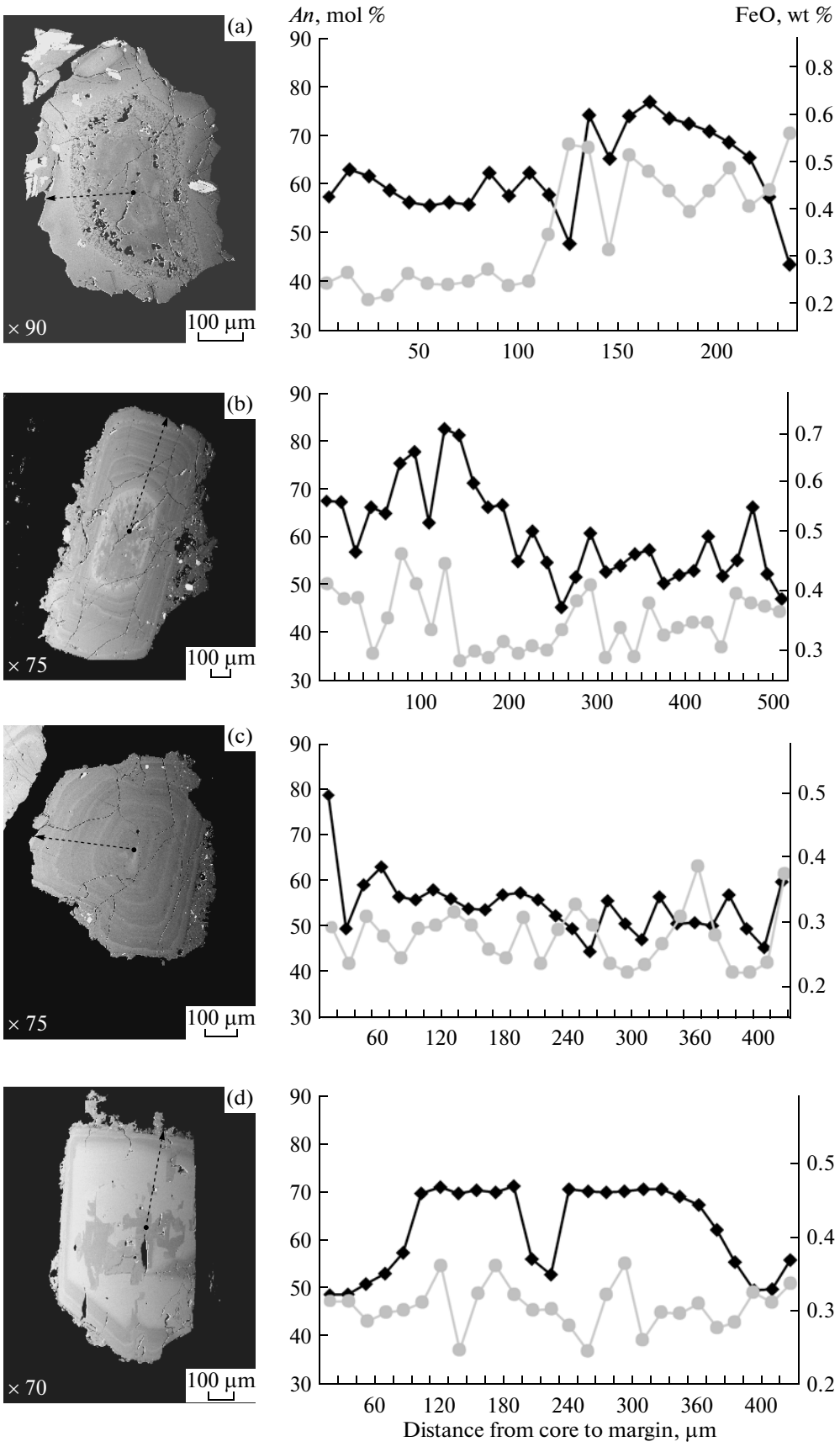
(a)
× 90
100 μm
(b)
× 75
100 μm
(c)
× 75
100 μm
(d)
× 70
100 μm
An, mol %
FeO, wt %
Distance from core to margin, μm

COMPOSITION OF ROCK-FORMING MINERALS

Plagioclase

Plagioclase is the predominant phenocryst mineral in all of the examined rock varieties from Young Shiveluch volcano, except only for the olivine–hornblende plagioclase-bearing andesites and olivine–clinopyroxene–hornblende phlogopite-bearing basalts. The composition of phenocryst cores varies from An_{32} to An_{88}. A complex zoning, diverse structures, and significant variations in the composition of phenocryst cores are typical of plagioclase in the andesite and basaltic andesite lavas. Resorbed and melted-through cores, intermediate, and outer zones and the contrasting normal, reversed, or oscillatory zoning are typical of plagioclase from Young Shiveluch. Drastic compositional changes, which are often marked by resorption zones with abundant melt inclusions are typical of boundaries between the cores and outer zones (Fig. 5a) and of intermediate zones. The plagioclase typically has a patchy core of the composition of approximately 80 mol % *An* (Fig. 5b), with thin cyclic zoning (Fig. 5c), and a sodic core rounded by melting (Fig. 5d), which has a reversed zoning. All of the aforementioned zoning types can occur in phenocrysts contained in the same sample, as is pronounced most clearly in andesites from the modern extrusion dome and northeast-trending lava flows in the northeastern sector of Young Shiveluch (Table 3).

The statistical variations in the composition of the cores and intermediate zones of the plagioclase phenocrysts suggest an admixture of andesite material in the basaltic andesite and an admixture of basaltic andesite in the andesite (Figs. 6a, 6b). A bimodal composition distribution is typical of plagioclase in both the andesite and the basaltic andesite lavas. The phenocrysts of the andesites are strongly predominated by labradorite $An_{48–56}$. The phenocrysts in basaltic andesites are dominated by labradorite–bytownite $An_{68–76}$, but these rocks additionally contain numerous phenocrysts of the $An_{48–56}$ composition.

Variations in the trace-element composition of plagioclase provide the most interesting information on magma mixing during the origin of the rock series of Young Shiveluch. As can be seen in Fig. 7, calcic plagioclase in the *Ol–Cpx–Pl* basaltic andesites bears FeO concentrations two and more times higher than those in phenocrysts in the *Hbl–Pl* basalts. The composition data points of plagioclase from the *Ol–Px–Pl* ± *Hbl* rocks (sample 7487), which are reliably identified as intermediate hybrid varieties, compose two clearly defined groups corresponding to basaltic andesite and andesite lavas.

Amphibole

Amphibole. Amphibole phenocrysts occur in all rock varieties from Young Shiveluch in amounts ranging from single grains in the *Ol–Cpx–Pl* basaltic andesite to 7–25 vol % in the more silicic rocks. In the *Hbl–Pl* andesites, brown hornblende occurs as prismatic crystals (up to 2–3 mm), which often contain opacite rims in the margins and often contain abundant plagioclase inclusions of the composition $An_{48–63}$. The basaltic andesite and hybrid lavas of Young Shiveluch contain amphibole in the form of rare wedge-shaped phenocrysts that are almost completely opacitized or replaced by aggregates of pyroxene, plagioclase, and ore mineral. Phenocrysts in the *Ol–Hbl* ± *Pl* andesites are pargasite hornblende, whose cores often preserve olivine and, more rarely, clinopyroxene relics.

The phenocrysts examined in the rocks are classed with calcic amphibole and define two compact groups in the classification diagrams. These groups correspond to pargasite and the magnesian hornblende–tschermakite series (Figs. 8a, 8b). In the Al_2O_3 and Na_2O vs. Mg# plots (Figs. 8c, 8d), amphiboles from Young Shiveluch define two pronounced trends corresponding to amphiboles of distinct petrographic types. The pargasite amphibole in the *Ol–Hbl* ± *Pl* andesites have fairly stable Al_2O_3 concentrations of 11.8–15.2 wt %, 2.0–2.5 wt % Na_2O, and low concentrations of TiO_2 of 0.9–1.7 wt %, which are not correlated with the Mg# (60–80 mol %). The Al_2O_3 and Na_2O concentrations in the cores of hornblende phenocrysts in the *Hbl–Pl* andesite broadly vary (6.6–13.6 wt % Al_2O_3 and 1.4–2.7 wt % Na_2O) and are negatively correlated with the Mg# of the mineral (Figs. 8c, 8d). Within the range of its Mg# = 65–75, the hornblende has high TiO_2 concentrations of up to 2.5 wt %. At the predominance of cores and unzoned phenocrysts with 8–11 wt % Al_2O_3, some samples of the *Hbl–Pl* andesite additionally contain amphibole with aluminous cores of composition close to that of amphibole in the *Ol–Hbl* ± *Pl* andesite. The Al_2O_3, Na_2O, and TiO_2 concentrations and in Mg# of zonal amphibole phenocrysts in the *Hbl–Pl* andesite also vary (Table 4). The most typical zoning is pronounced as a decrease in the concentrations of these components at increasing Mg# from the cores to margins of the grains. Modern extrusive lavas (samples 7433, 7515, 7515-1, and 7522) occasionally contain amphibole with reversed

Fig. 5. Zoning of plagioclase phenocrysts in the lava of the modern extrusive dome (sample 7515-1). (a) Plagioclase with reversed zoning, whose core and more calcic margin are separated by a broad resorption zone with abundant melt inclusions; (b) plagioclase with a patchy deanorthitized core; (c) plagioclase with thin oscillatory zoning and a relict calcic core; (d) plagioclase with a resorbed sodic core. The heavy line with diamonds shows the variations in the concentration of the anorthite end member, the gray line shows the variations in the FeO concentration across the crystal. The profile line is shown in the images by a dashed line with an arrowhead.

Table 3. Representative analyses (wt %) of plagioclase from the lava complex of Young Shiveluch volcano

Component	Sample 7496a												
	c	i	i	i	m	c	m	c	i	m	mi	mi	mi
SiO_2	58.30	51.19	59.35	55.49	56.87	51.65	58.19	58.03	52.87	58.14	53.92	55.97	50.85
TiO_2	0.00	0.00	0.00	0.00	0.01	0.00	0.04	0.03	0.00	0.03	0.05	0.07	0.00
Al_2O_3	25.19	29.59	24.21	26.48	26.86	29.25	24.97	25.37	28.99	25.67	29.25	27.69	30.36
FeO	0.37	0.31	0.38	0.46	0.50	0.53	0.69	0.33	0.39	0.41	1.06	1.02	1.05
MgO	0.00	0.00	0.00	0.00	0.00	0.00	0.00	0.00	0.00	0.00	0.03	0.00	0.01
CaO	7.60	13.33	7.00	9.76	10.03	13.22	8.20	8.96	12.41	8.35	12.80	10.32	14.36
Na_2O	6.70	3.95	7.01	5.66	4.25	3.59	5.96	5.99	3.96	5.56	3.84	5.45	3.40
K_2O	0.33	0.17	0.40	0.32	0.33	0.14	0.45	0.36	0.20	0.33	0.33	0.48	0.11
Total	98.51	98.55	98.37	98.21	98.85	98.37	98.54	99.08	98.82	98.49	101.28	101.00	100.13
An, mol %	48.76	73.90	45.59	59.14	66.45	75.55	53.56	55.66	72.42	55.75	73.64	61.36	78.01
	Sample 7487												
	c	i	m	c	m	c	i	i	i	m	mi	mi	mi
SiO_2	60.45	59.07	52.04	52.44	58.76	57.82	54.05	58.98	51.22	58.73	50.87	52.66	50.04
TiO_2	0.00	0.00	0.00	0.00	0.00	0.00	0.00	0.00	0.00	0.00	0.03	0.02	0.00
Al_2O_3	23.49	24.46	28.84	28.75	24.69	25.99	28.21	24.39	30.14	24.86	29.80	28.40	28.72
FeO	0.44	0.36	0.95	0.46	0.46	0.44	0.38	0.41	0.35	0.41	0.94	1.08	1.25
MgO	0.02	0.01	0.01	0.02	0.00	0.02	0.02	0.00	0.01	0.00	0.00	0.03	0.00
CaO	6.87	7.50	13.43	13.13	8.02	8.81	11.41	7.37	13.46	7.38	13.41	12.18	13.44
Na_2O	7.13	6.88	3.16	4.15	7.09	6.08	4.70	6.60	3.37	6.95	3.74	4.68	3.68
K_2O	0.54	0.50	0.22	0.17	0.56	0.25	0.19	0.67	0.13	0.36	0.21	0.26	0.21
Total	98.94	98.77	98.65	99.11	99.60	99.41	98.96	98.42	98.68	98.69	98.99	99.31	97.34
An, mol %	44.70	47.77	78.09	72.64	48.71	54.88	67.07	48.39	77.03	47.11	75.08	68.62	75.43
	Sample 7433								Sample 7515				
	c	m	c	i	m	c	i	m	c	i	i	i	m
SiO_2	49.79	55.94	50.88	57.80	57.25	56.96	52.54	57.64	59.95	53.32	58.45	53.65	59.57
TiO_2	0.00	0.00	0.00	0.00	0.00	0.00	0.00	0.00	0.08	0.06	0.08	0.06	0.09
Al_2O_3	33.44	27.63	30.56	25.83	26.83	25.90	30.14	26.68	26.45	30.73	27.39	30.97	26.85
FeO	0.59	0.56	0.28	0.33	0.45	0.37	0.24	0.31	0.32	0.31	0.31	0.30	0.32
MgO	0.00	0.00	0.00	0.00	0.00	0.00	0.00	0.00	0.00	0.00	0.00	0.00	0.00
CaO	16.77	9.88	13.48	7.84	9.32	7.03	12.56	8.75	7.22	12.03	8.19	12.25	7.42
Na_2O	1.78	5.51	3.96	6.99	6.90	8.26	4.69	7.00	6.19	4.24	5.93	4.14	6.06
K_2O	0.05	0.30	0.00	0.00	0.00	0.00	0.00	0.00	0.32	0.14	0.28	0.13	0.30
Total	100.21	99.84	99.23	98.79	100.79	98.57	100.3	100.42	100.53	100.84	100.63	101.50	100.60
An, mol %	88.78	60.10	74.09	48.47	53.15	41.65	69.22	51.22	49.47	70.43	53.69	71.29	50.68

Note: In Tables 3–6, the geological setting and types of samples are the same as in Table 1; c—core, i—intermediate zone, m—margin, mi—microlite.

zoning: the Mg# decreases and the Al_2O_3, Na_2O, and TiO_2 concentrations increase toward the margins.

Pyroxenes

The basaltic andesite lavas contain 7–10 vol % clinopyroxene. Clinopyroxene occurs in the andesites as single resorbed phenocrysts and rare microlites, and the content of orthopyroxene is 2–3 % of the rock by volume. The composition of clinopyroxene phenocrysts in the basaltic andesites corresponds to augite and diopside-augite $Wo_{42-47}En_{40-48}Fs_{6-14}$ (Fig. 9a, Table 5). The range of the Mg# of phenocryst cores is 75.7–88.7. The histograms display two clearly pronounced maxima of Mg# at 80–84 and 86–88 (Fig. 9b). As the Mg# of the clinopyroxene decreases, the TiO_2 and Al_2O_3 systematically increase (Figs. 10a, 10b), whereas the Cr concentrations drastically decrease (Fig. 9c).

The phenocrysts mostly have a normal zoning, with Mg# decreasing from cores to margins. A well pronounced reversed zoning was detected in clinopyroxene from the *Ol–Px–Pl* ± *Hbl* andesite (sample 7487, Table 5). The cores of these phenocrysts have Mg# = 78–79, and their margins display Mg# = 81–85. The rare clinopyroxene phenocrysts and microlites of the andesite lavas have the

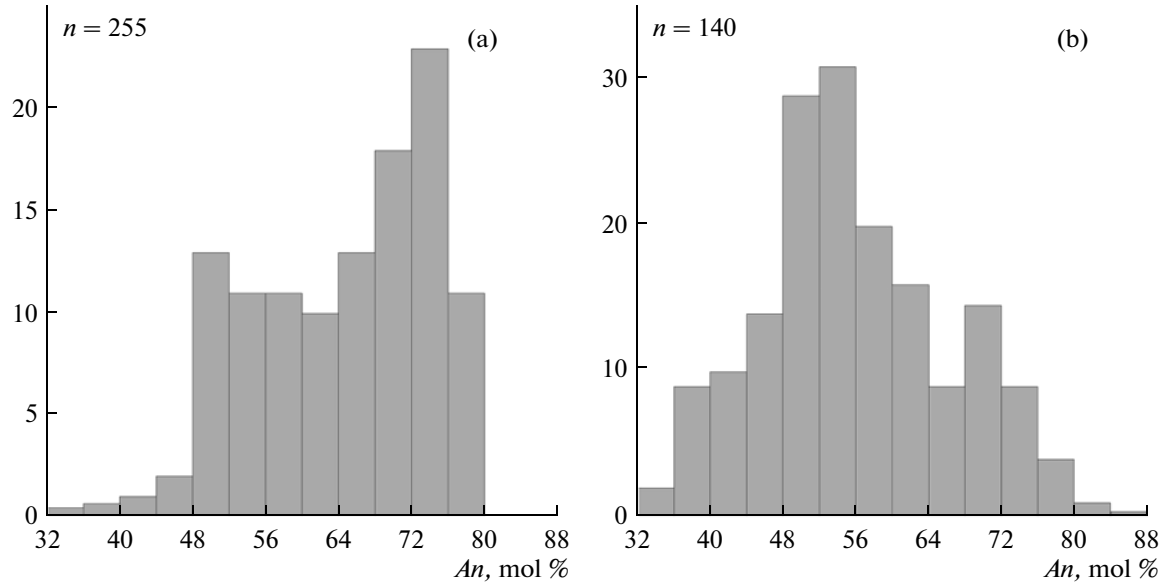

Fig. 6. Composition of plagioclase cores and intermediate zones in (a) andesite and (b) basaltic andesite lavas of Young Shiveluch volcano.

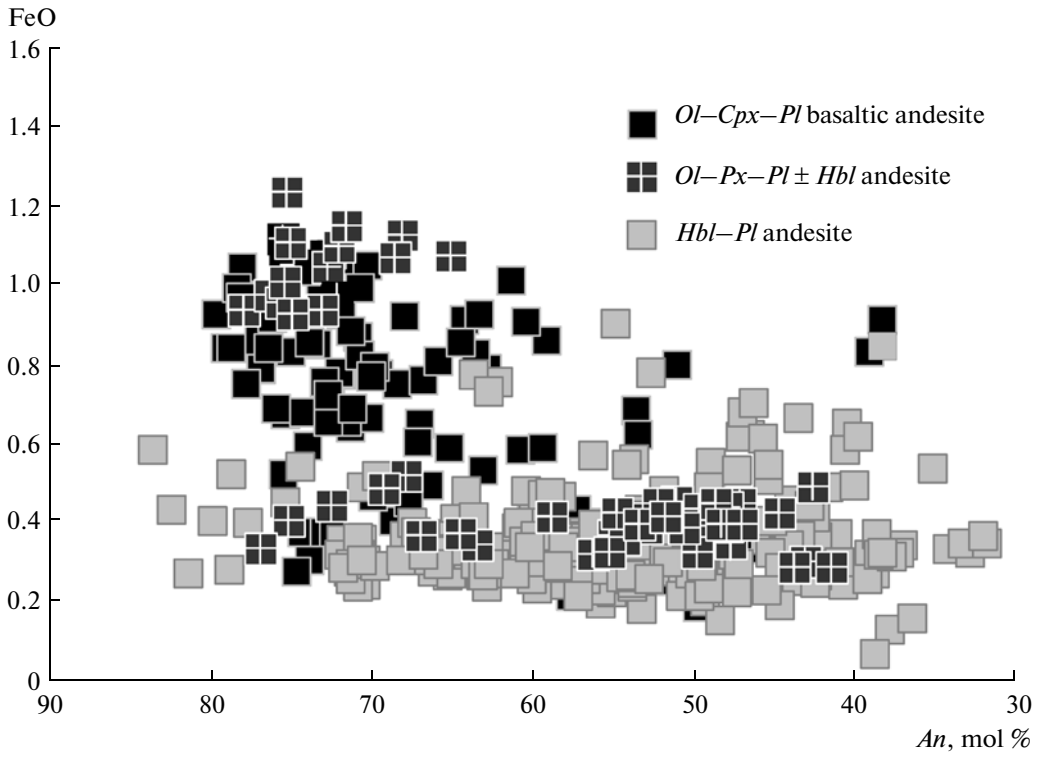

Fig. 7. Variations in the FeO concentration vs. anorthite content in plagioclase from various petrographic rock types of Young Shiveluch volcano.

composition $Wo_{39–40}En_{44–45}Fs_{15–16}$ and compositionally evolve toward subcalcic augite and pigeonite.

The orthopyroxene ($En_{64–67}Fs_{30–34}Wo_{3–2}$) occurs as prismatic grains ranging from a few fractions of a millimeter to 1 mm. The Mg# of orthopyroxene phenocrysts in the andesite lavas varies from 69 to 76. High-Mg orthopyroxene (Mg# = 80–85) was found only in reaction rims around olivine. The modern extrusive lavas contain crystals with reversed zoning, whose outer zones

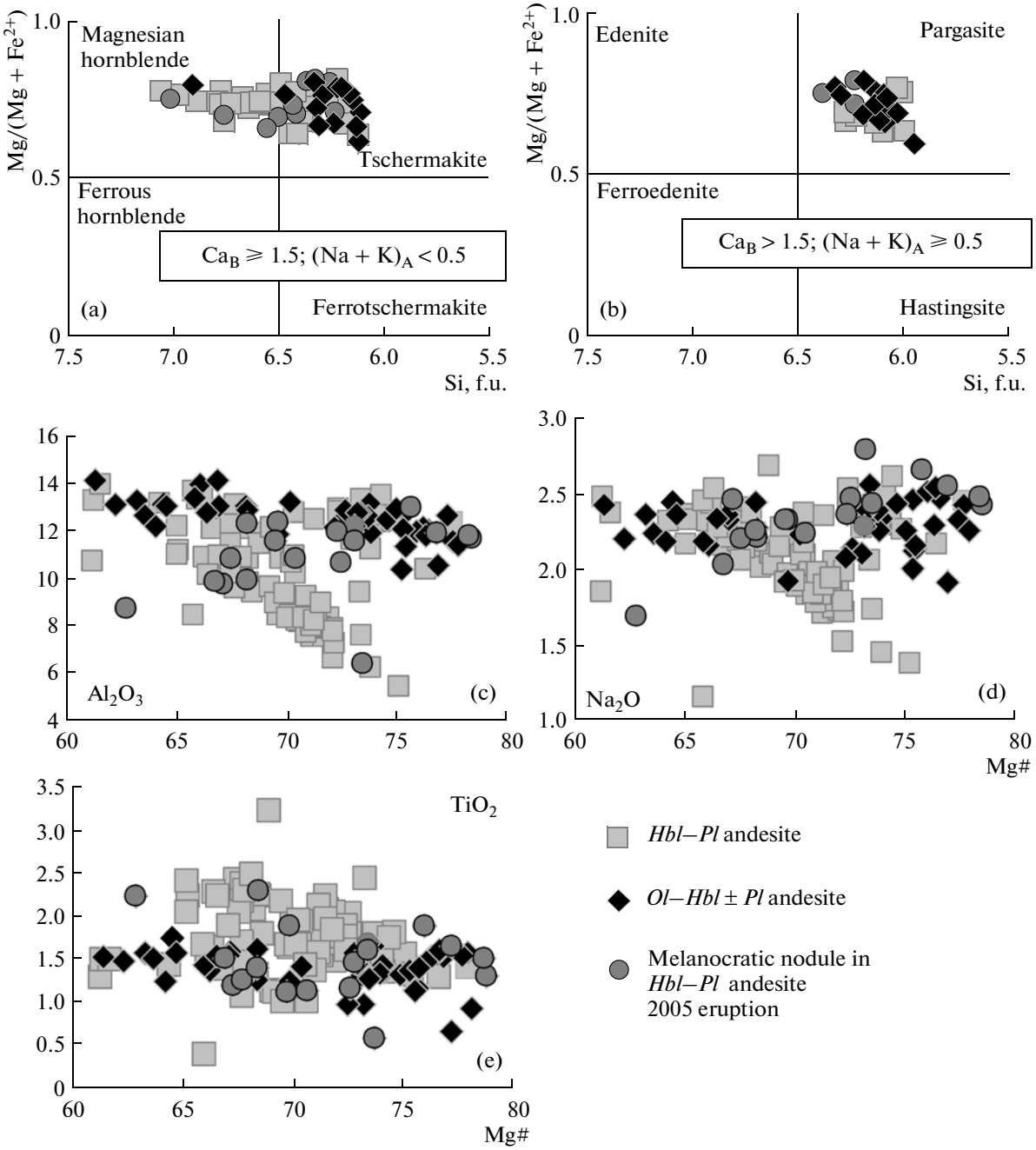

Fig. 8. (a, b) Systematics of amphibole in various petrographic rock types of Young Shiveluch volcano; variations in the (c) Al_2O_3, (d) Na_2O, and (e) TiO_2 concentrations in the cores of amphibole phenocrysts vs. their Mg#.

are richer in Ca and have a higher Mg# of 72–74 than the cores of the phenocrysts (Mg# = 69–70).

Olivine

Olivine is contained in all lava types in amounts ranging from 5–7 vol % in the basaltic andesite to single resorbed grains or grains surrounded by *Px–Hbl–Mt* rims in the silicic lavas. The most euhedral crystals were found in the *Ol–Px–Pl* ± *Hbl* basaltic andesite and andesite at the northeastern slope. Olivine in the heterotaxitic lavas is corroded and is often overgrown by granular pyroxene aggregates. Rare olivine phenocrysts in the *Ol–Hbl* ± *Pl* andesite are rimmed or surrounded by amphibole grains.

The overall range of the Mg# of the cores of olivine phenocrysts in lavas at Young Shiveluch is $Fo_{84–92}$ (Figs. 11a, 11b, Table 6). The most magnesian olivine $Fo_{90–92}$ was found in a melanocratic nodule (sample 7499-4) in andesite of the 2005 eruption. The composition of olivine in the nodule is close to that of the most magnesian olivine documented at this volcano

Table 4. Representative analyses (wt %) of amphiboles from lavas of Young Shiveluch volcano

Component	Sample 7522											
	c	i	m	c	i	m	c	m	c	m	c	m
SiO_2	46.81	44.01	46.95	43.72	43.02	47.29	43.62	48.11	43.67	47.82	47.42	44.05
TiO_2	1.42	2.16	0.99	1.46	2.39	2.03	2.22	1.43	2.03	1.75	1.76	2.43
Al_2O_3	9.43	11.46	10.20	13.08	12.19	7.86	12.45	7.61	11.02	7.24	8.20	11.63
FeO	10.68	12.41	11.61	11.98	13.15	11.28	10.71	10.70	13.34	11.18	11.70	10.06
MnO	0.28	0.24	0.32	0.32	0.36	0.32	0.18	0.28	0.31	0.31	0.29	0.19
MgO	16.67	14.54	15.64	14.15	13.79	16.14	15.05	16.79	13.97	16.42	15.81	15.41
CaO	10.97	11.42	11.27	11.61	11.63	11.63	12.06	11.49	11.71	11.60	11.45	12.40
Na_2O	2.06	2.41	2.10	2.32	2.33	1.91	2.36	1.74	2.17	1.72	1.84	2.28
K_2O	0.23	0.45	0.23	0.49	0.51	0.33	0.47	0.30	0.62	0.29	0.38	0.49
Cr_2O_3	0.16	0.26	0.13	0.54	0.02	0.01	0.13	0.06	0.01	0.00	0.16	0.28
Total	98.71	99.37	99.43	99.68	99.39	98.79	99.26	98.51	98.85	98.33	99.01	98.87
Mg#	73.56	67.62	70.60	67.80	65.15	71.83	71.47	73.64	65.12	72.36	70.66	73.19
	Sample 7516-1											
	c	i	i	m	c	i	m	c	i	m	c	m
SiO_2	42.37	44.69	43.43	44.33	40.87	43.17	42.63	43.08	42.2	43.04	43.96	41.86
TiO_2	1.74	1.34	1.25	1.51	1.47	1.42	1.08	1.64	1.53	1.56	1.35	1.52
Al_2O_3	13.09	11.90	13.06	12.04	15.21	13.14	12.91	12.74	14.11	13.05	12.93	14.13
FeO	13.13	10.11	12.34	9.21	15.26	9.85	16.04	10.21	12.08	13.25	9.32	14.18
MnO	0.27	0.16	0.16	0.15	0.25	0.12	0.48	0.11	0.20	0.24	0.15	0.24
MgO	13.38	16.2	14.91	17.04	11.12	15.72	12.19	15.94	13.77	13.6	15.86	12.63
CaO	11.63	11.51	11.35	11.36	11.79	11.78	10.79	11.82	12.00	11.57	12.17	11.63
Na_2O	2.45	2.34	2.45	2.48	2.22	2.26	2.08	2.57	2.37	2.37	2.26	2.43
K_2O	0.47	0.39	0.40	0.43	0.62	0.59	0.40	0.60	0.61	0.45	0.60	0.50
Cr_2O_3	0.05	0.14	0.00	0.12	0.00	0.02	0.00	0.03	0.10	0.12	0.16	0.00
Total	98.59	98.78	99.35	98.67	98.8	98.07	98.6	98.74	98.98	99.25	98.75	99.12
Mg#	64.49	74.07	68.29	76.73	56.5	73.99	57.53	73.56	67.02	64.66	75.21	61.35
	Sample 7500						Sample 7499-4					
	c	m	c	m	c	m	c	m	c	m	mi	mi
SiO_2	44.43	45.48	44.79	47.83	44.27	43.08	44.22	48.51	45.77	44.85	44.58	44.46
TiO_2	2.41	2.22	2.36	1.79	1.37	1.71	1.88	1.18	1.50	1.63	1.11	1.39
Al_2O_3	10.54	9.78	10.09	7.55	12.08	12.74	12.98	9.74	9.86	11.91	11.58	12.29
FeO	12.63	12.40	12.42	11.57	12.75	11.51	9.02	12.54	13.12	9.07	11.78	12.11
MnO	0.32	0.21	0.30	0.23	0.29	0.12	0.06	0.41	0.25	0.11	0.16	0.27
MgO	14.61	15.07	14.56	16.17	14.37	15.43	15.96	14.44	14.84	17.13	15.18	14.66
CaO	11.51	11.66	11.53	11.66	11.75	11.79	12.18	10.87	11.38	11.68	11.89	11.67
Na_2O	2.29	2.11	2.17	1.71	2.16	2.38	2.67	2.47	2.04	2.56	2.33	2.26
K_2O	0.47	0.46	0.46	0.32	0.45	0.54	0.25	0.42	0.41	0.23	0.22	0.59
Cr_2O_3	0.02	0.05	0.09	0.03	0.00	0.01	0.06	0.10	0.13	0.07	0.52	0.16
Total	99.23	99.44	98.76	98.86	99.49	99.31	99.28	100.68	99.31	99.24	99.35	99.86
Mg#	67.34	68.42	67.63	71.36	66.77	70.50	75.93	67.24	66.84	77.10	69.67	68.33

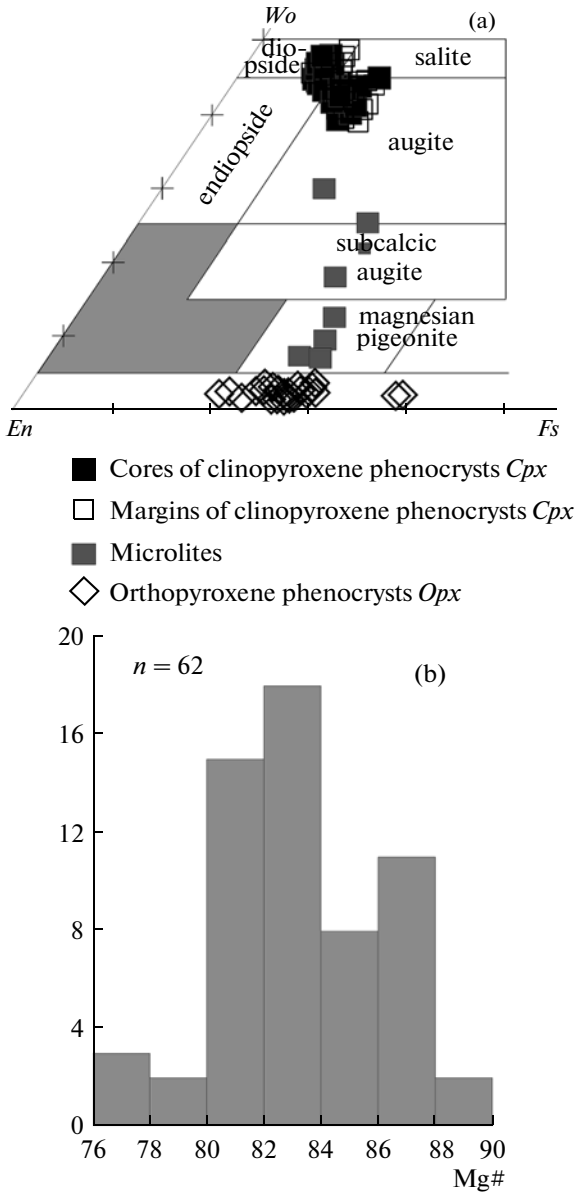

Fig. 9. (a) Systematics of pyroxene phenocrysts in andesitic basalt lavas of Young Shiveluch volcano and (b) distribution of the Mg# of the cores of pyroxene phenocrysts in the basaltic andesite lavas.

(Volynets et al., 1997) in tephra of *Ol–Cpx–Hbl ± Phl* basalt of the eruption at 3600 ^{14}C years. The composition of olivine phenocrysts in the andesite and basaltic andesite lavas is somewhat more ferrous ($Fo_{84–89.5}$), at the strong predominance of $Fo_{86–88}$ (Fig. 11). All phenocrysts in the andesite and basaltic andesite lavas display a normal zoning, with the outermost zones having the composition $Fo_{73–85}$. As the Mg# of olivine decreases, its CaO concentrations remains practically unchanged (0.08–0.12 wt %), the MnO concentration increases (0.1–0.25 wt %), and that of NiO decreases (0.5–0.1 wt %). Olivine of the composition $Fo_{88–90}$ in the hybrid lavas (sample 7487) is richer in NiO than olivine in the melanocratic nodule and in the *Ol–Hbl–Cpx ± Phl* basalts.

Olivine phenocrysts contain small Cr-spinel inclusions, which sometimes occur as abundant filamentous accumulations. The value of the Cr# = 65.4–76.2 and the concentration of TiO_2 = 0.26–1.02 wt % of the Cr-spinel of Young Shiveluch are close to those of this mineral in basalt from Klyuchevskoi volcano (Khubunaya et al., 1993), but the former mineral shows broad Mg# variations of 29–61 (Table 7). The compositional data points of the Young Shiveluch spinel, which coexists with magnesian olivine (Fig. 12), plot within the field of mantle rocks (Arai, 1994), and this suggests that the mineral crystallized from primitive melts close to the parental mantle magmas in composition.

PETROCHEMISTRY

The composition of rocks of the Young Shiveluch lava complex is reported in Table 2. Most of the lavas have compositions of magnesian andesite and basaltic andesite with 55.0–63.5 wt % SiO_2 and Mg# = 55.5–68.9 mol % and affiliate with the moderately potassic calc–alkaline series (Fig. 13). The most mafic rocks found in the lava complex are *Ol–Cpx–Hbl ± Phl* basalts (50.5–51.0 wt % SiO_2 and Mg# = 69.4–71.7 mol %), which affiliate (similar to the tephra of the 3600 ^{14}C years eruption) to the highly potassic series (Fig. 13b).

Variations in the contents of major and trace elements in Young Shiveluch lavas are exhibited in Figs. 14 and 15. A decrease in the MgO concentration of the rocks from 9.43 to 3.32 wt % is associated with enrichment in Al_2O_3 (from 15.34 to 16.89 wt %), Na_2O (from 3.20 to 4.90 wt %), and K_2O (from 0.73 to 1.49 wt %). The concentrations of TiO_2, FeO, CaO, and P_2O_5 slightly increase or remain unchanged at MgO decreasing to approximately 4–5 wt % and are lower in the more evolved rocks (0.80–0.48 wt % TiO_2, 8.29–4.28 wt % FeO, 8.25–5.38 wt % CaO, and 0.25–0.06 wt % P_2O_5). An analogous behavior is typical of V (233–106 ppm), Zn (82–51 ppm), and Y (25–8 ppm). Within the range of MgO = 9.5–5 wt %, the rocks are significantly depleted in Cr (563–167 ppm) and Ni (173–31 ppm). The Cr and Ni concentrations in the lavas with MgO < 5 wt % are 154–94 and 39–14 ppm, respectively. The distribution in the Sr and Ga concentrations is analogous to that of Al: a decrease in the MgO content is typically associated with the accumulation of these elements (14–20 ppm Ga and 328–654 ppm Sr). The concentrations of incompatible elements (Ba, Rb, and Zr) of the rocks increase by a factor of approximately 1.5 with a decrease in the MgO concentration.

An anomalous enrichment in Sr (1004 ppm) and Ba (608 ppm) was detected in the extrusion of Mount Karan. The *Ol–Cpx–Hbl ± Phl* basalts plot far away from the trends of Young Shiveluch lavas because of their elevated concentrations of K_2O (1.93 wt %), P_2O_5

Table 5. Representative analyses (wt %) of pyroxenes from rocks of the lava complex of Young Shiveluch volcano

Component	Sample 7496						Sample 7487					
	Cpx			*Opx*			*Cpx*					
	c	c	m	c	c	m	c	m	c	m	c	m
SiO_2	51.23	51.92	49.97	53.36	54.83	54.85	52.57	50.6	53.11	50.13	52.27	47.79
TiO_2	0.58	0.57	0.54	0.16	0.13	0.08	0.19	0.55	0.23	0.68	0.29	1.39
Al_2O_3	2.54	2.32	3.33	0.81	0.52	0.41	1.08	3.85	0.93	3.80	1.99	6.45
FeO	4.71	4.68	8.41	16.28	16.42	18.04	7.42	6.15	6.97	5.87	5.57	9.39
MnO	0.12	0.15	0.30	0.50	0.55	1.06	0.20	0.01	0.15	0.02	0.02	0.08
MgO	16.14	16.59	15.05	26.42	26.82	25.28	14.77	15.00	14.82	15.62	16.67	13.70
CaO	22.44	22.03	21.12	1.03	0.81	0.86	22.01	22.10	22.56	21.94	21.89	21.03
Na_2O	0.28	0.26	0.21	0.03	0.06	0.00	0.00	0.03	0.32	0.00	0.00	0.00
Cr_2O_3	0.67	0.42	0.04	0.00	0.00	0.00	0.00	0.14	0.00	0.23	0.32	0.00
Total	98.72	98.95	98.98	98.61	100.2	100.58	98.25	98.45	99.12	98.29	99.04	99.88
Mg#	87.16	87.53	77.99	76.27	76.39	73.51	79.75	82.85	80.82	84.06	85.57	74.29
	Sample 7487								Sample 7499-4			
	Cpx		*Opx*						*Cpx*			
	mi	mi	c	m	c	m	mi	mi	c	m	c	m
SiO_2	51.47	50.25	54.82	54.79	54.97	55.01	52.98	52.18	53.05	51.99	51.23	52.71
TiO_2	0.35	0.52	0.10	0.09	0.06	0.06	0.29	0.52	0.14	0.20	0.39	0.14
Al_2O_3	2.48	3.69	0.38	0.77	0.29	0.34	1.56	1.94	1.60	1.17	2.84	1.18
FeO	5.48	5.84	17.16	17.89	17.51	17.23	14.66	10.64	4.29	9.74	5.66	8.25
MnO	0.04	0.03	0.61	0.66	1.01	0.94	0.51	0.30	0.00	0.52	0.01	0.32
MgO	16.33	15.21	26.17	25.36	25.74	26.32	24.64	18.93	16.98	15.66	15.28	14.01
CaO	22.23	22.06	0.88	0.94	0.79	0.67	1.74	14.48	22.21	19.56	22.62	21.8
Na_2O	0.05	1.68	0.00	0.00	0.00	0.00	0.00	0.00	0.03	0.02	0.00	0.08
Cr_2O_3	0.42	0.53	0.00	0.00	0.00	0.00	0.00	0.00	0.38	0.00	0.25	0.00
Total	98.88	99.83	100.13	100.53	100.39	100.61	96.39	99	98.7	98.88	98.29	98.51
Mg#	85.51	83.77	75.12	73.74	74.43	75.15	76.9	77.89	88.69	76.11	84.23	77.07
	Sample 7499-4					Sample 7433						
	Cpx		*Opx*			*Cpx*			*Opx*			
	c	m	c	m	at *Ol*	c	mi	mi	c	c	mi	mi
SiO_2	53.98	51.7	55.39	55.42	54.14	53.16	51.00	50.99	53.98	53.2	53.49	52.58
TiO_2	0.15	0.51	0.07	0.08	0.00	0.25	0.63	0.74	0.11	0.16	0.28	0.23
Al_2O_3	1.08	3.44	0.48	0.22	3.16	1.45	1.92	1.84	0.52	1.76	0.88	0.83
FeO	5.10	6.85	18.11	17.51	13.01	7.01	9.73	9.58	18.08	17.56	16.53	16.00
MnO	0.00	0.01	0.92	0.98	0.43	0.11	0.33	0.32	0.75	0.64	0.54	0.48
MgO	16.13	14.72	24.52	24.46	27.9	16.15	15.31	15.65	25.50	25.77	26.08	26.62
CaO	22.52	22.75	0.73	0.43	0.94	20.89	19.25	19.06	1.21	0.97	1.19	1.51
Na_2O	0.00	0.01	0.00	0.00	0.00	0.31	0.47	0.49	0.03	0.03	0.04	0.03
Cr_2O_3	0.01	0.03	0.00	0.00	0.00	0.00	0.00	0.00	0.00	0.00	0.00	0.00
Total	98.97	100.08	100.24	99.14	99.6	99.36	98.70	98.72	100.20	100.13	99.12	98.28
Mg#	86.23	80.98	72.84	73.44	80.94	82.03	75.70	76.39	73.64	74.40	75.76	76.72

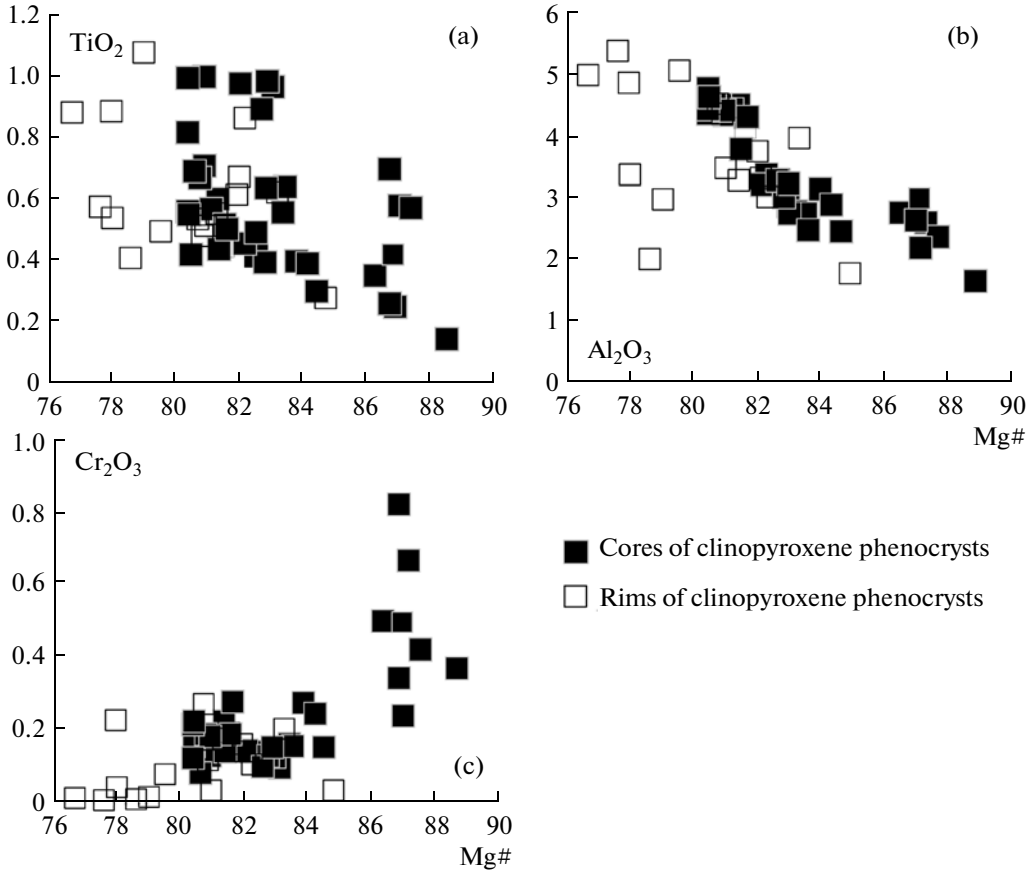

Fig. 10. Variations in the concentrations of (a) TiO_2, (b) Al_2O_3, and (c) Cr_2O_3 in clinopyroxene in basaltic andesite lavas of Young Shiveluch volcano depending on the Mg# of the clinopyroxene.

(0.41 wt %), Rb (45 ppm), Ba (475 ppm), Sr (485 ppm), and Y (22 ppm).

DISCUSSION

Role of Crystallization Differentiation

The compositional data points of the lava complex and proximal pyroclastic deposits of Young Shiveluch volcano plot along the same evolutionary trends with respect to MgO. The possible parental magma can correlate in composition to the basaltic tephra of the eruption at 7600 ^{14}C years (Volynets et al., 1997; Ponomareva et al., 2007). This rock has the maximum concentrations of mafic components (Mg, Fe, Cr, and Ni) and minimum concentrations of incompatible lithophile elements (K, Rb, and Ba) among all rocks composing the Young Shiveluch series (Figs. 13, 14). The trend is controlled predominantly by the crystallization differentiation of Fe–Mg silicates and oxides: the *Ol* ± *Spl* + *Cpx* assemblage in the basaltic andesite lavas gave way to the *Hbl* ± *Px* + *Mt* assemblage in the andesites, which predetermined a systematic decrease in the concentrations of CaO, FeO, MnO, TiO_2, Cr, Ni, and V at an increase in the concentrations of SiO_2, Na_2O, K_2O, Rb, and Ba at decrease MgO concentrations of the rocks. The crystallization of apatite on the liquidus took place at a MgO concentrations of approximately 4–5 wt %, as can be seen from the kink on the P_2O_5 trend with a decrease MgO.

Paradoxically, the fractionation trend of rocks of Young Shiveluch at the first glance seems not to indicate that the rocks contain plagioclase as the predominant mineral of most of the rocks (except only for the *Ol–Hb*l ± *Pl* andesites and *Ol–Cpx–Hbl* ± *Phl* basalts), which accounts for half to one-third of all phenocrysts. The enrichment in Al_2O_3 and Sr with an increase in the SiO_2 concentration and a decrease in the MgO concentration of the magmas (Figs. 14, 15) seems to be at variance with the massive crystallization of plagioclase and data on the composition of melt inclusions in the andesites, whose Sr concentrations are no higher than 360 ppm and are negatively correlated with SiO_2 (Tolstykh et al., 2003; Humphreys et al., 2008).

This fact testifies that the incomplete removal of plagioclase crystals from the crystallizing melt could notably affect the bulk composition of the erupted magmas and maintain the bulk Al_2O_3 and Sr contents of the magmas at a higher level than that of the equilibrium melt during each next fractionation stage. The clearly pronounced and diverse zoning of plagioclase crystals occurring in a single sample (Fig. 5) corrobo-

Table 6. Representative analyses (wt %) of olivine phenocrysts from lavas of Young Shiveluch volcano

Component	Sample 7482				Sample 7487							
	c	m	c	m	c	c	c	m	c	m	c	m
SiO_2	40.97	39.37	40.77	39.27	41.03	41.33	41.15	40.89	41.06	39.75	40.59	40.6
FeO	11.87	19.02	12.00	19.78	10.27	10.72	10.74	13.14	10.79	17.93	13.71	15.39
MnO	0.20	0.38	0.20	0.367	0.14	0.16	0.15	0.20	0.15	0.35	0.23	0.27
MgO	48.08	42.3	47.98	41.69	48.99	48.78	48.43	46.88	48.41	42.83	46.56	45.3
CaO	0.12	0.13	0.12	0.13	0.09	0.09	0.10	0.16	0.09	0.10	0.11	0.11
NiO	0.15	0.07	0.13	0.05	0.43	0.38	0.40	0.23	0.45	0.07	0.24	0.12
Cr_2O_3	0.04	0.01	0.03	0.01	0.04	0.02	0.03	0.03	0.03	0.01	0.02	0.00
Total	101.44	101.28	101.23	101.3	101	101.48	100.99	101.49	100.99	101.05	101.48	101.8
Fo, mol %	87.83	79.86	87.7	78.98	89.47	89.02	88.94	86.41	88.88	80.98	85.82	83.99
	Sample 7516-1				Sample 7499-4							
	c	m	c	m	c	m	c	m	c	m	c	m
SiO_2	40.92	39.94	40.74	40.41	41.6	41.43	41.6	40.37	41.24	40.88	41.34	40.72
FeO	10.50	15.50	12.72	14.08	7.81	7.94	8.10	15.34	9.20	11.07	9.25	13.3
MnO	0.13	0.31	0.17	0.21	0.11	0.1	0.12	0.34	0.13	0.15	0.13	0.21
MgO	48.34	45.22	47.37	46.11	50.66	50.95	50.76	45.07	49.91	48.67	49.5	46.61
CaO	0.32	0.06	0.08	0.07	0.10	0.08	0.10	0.12	0.09	0.11	0.15	0.12
NiO	0.33	0.26	0.28	0.21	0.44	0.53	0.46	0.13	0.45	0.27	0.50	0.14
Cr_2O_3	0.25	0.01	0.01	0.01	0.05	0.05	0.06	0.01	0.03	0.05	0.55	0.02
Total	100.79	101.29	101.38	101.1	100.79	101.09	101.19	101.37	101.05	101.22	101.43	101.12
Fo, mol %	89.14	83.87	86.91	85.37	92.04	91.96	91.78	83.97	90.62	88.68	90.51	86.21
	Sample 7499-4			Sample K1-18b								
	c	m	c	c	c	c	c	c	c	c	c	c
SiO_2	41.42	40.55	41.18	40.77	40.59	40.49	40.43	40.24	40.48	40.14	39.81	39.96
FeO	10.25	13.43	10.81	7.26	7.82	8.24	8.75	9.26	10.03	11.40	12.00	12.52
MnO	0.15	0.21	0.16	0.09	0.11	0.10	0.12	0.13	0.15	0.18	0.20	0.20
MgO	49.07	46.88	48.64	50.71	50.42	50.04	49.63	49.31	48.81	47.95	47.2	46.84
CaO	0.10	0.11	0.13	0.05	0.07	0.08	0.10	0.12	0.11	0.11	0.10	0.11
NiO	0.31	0.13	0.24	0.44	0.38	0.4	0.37	0.36	0.29	0.19	0.20	0.16
Cr_2O_3	0.04	0.03	0.03	0.06	0.07	0.05	0.05	0.04	0.04	0.04	0.03	0.02
Total	101.35	101.34	101.19	99.42	99.49	99.45	99.51	99.52	99.95	100.05	99.56	99.86
Fo, mol %	89.51	86.15	88.91	92.57	92.00	91.55	91.01	90.47	89.67	88.23	87.52	86.96

rate this hypothesis and implies that plagioclase resided for a long time (was recycled) in the magmas and interacted with melts of various composition. Conversely, complicated zoning is atypical of Fe–Mg silicates in the Young Shiveluch rocks. Having a higher density than plagioclase, these minerals (olivine, amphibole, and pyroxenes) could be more efficiently removed from the crystallizing system by gravitational

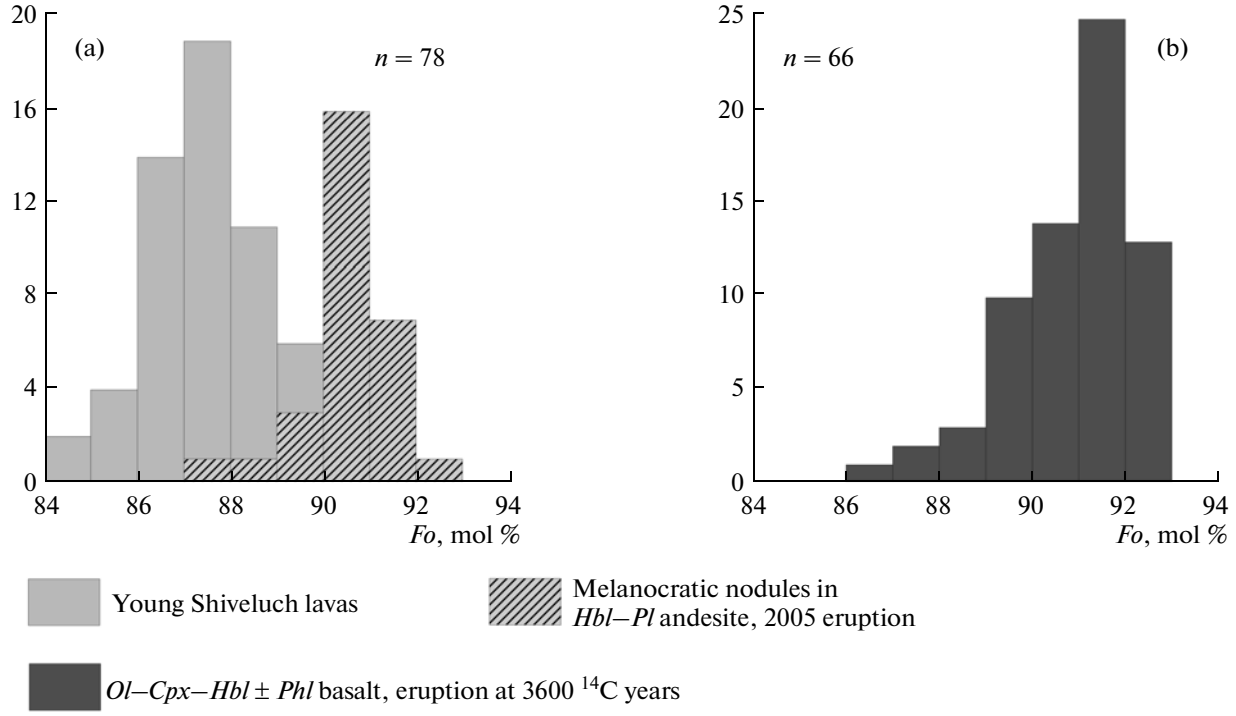
(a)
n = 78
Fo, mol %
(b)
n = 66
Fo, mol %
Young Shiveluch lavas
Melanocratic nodules in Hbl–Pl andesite, 2005 eruption
Ol–Cpx–Hbl ± Phl basalt, eruption at 3600 14C years

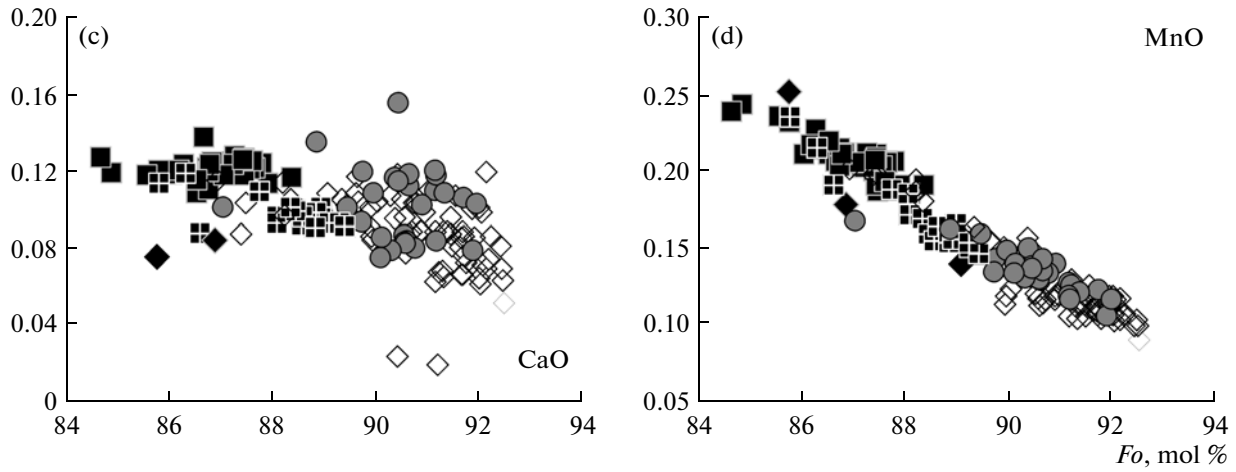
(c)
CaO
(d)
MnO
Fo, mol %

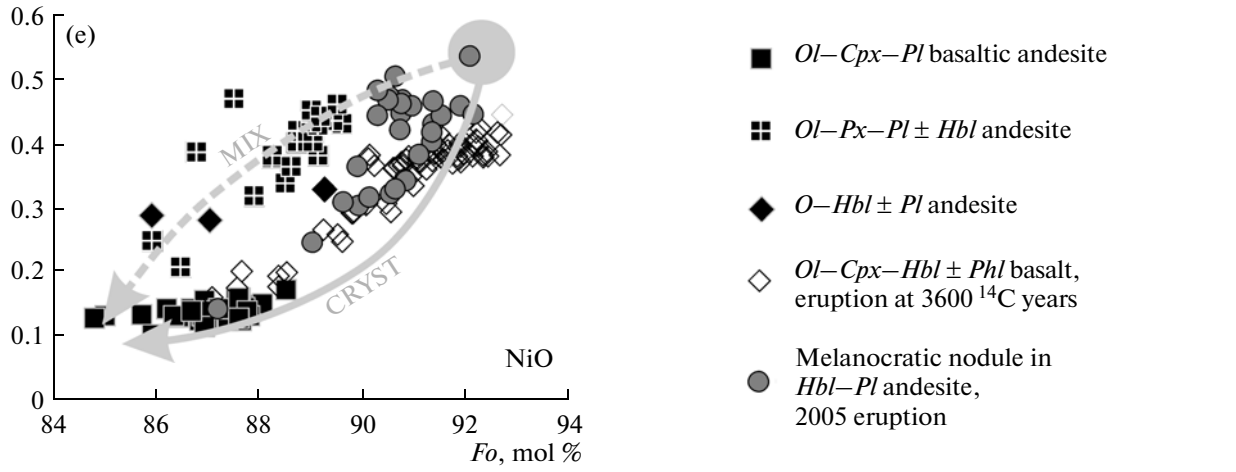
(e)
MIX
CRYST
NiO
Fo, mol %
Ol–Cpx–Pl basaltic andesite
Ol–Px–Pl ± Hbl andesite
O–Hbl ± Pl andesite
Ol–Cpx–Hbl ± Phl basalt, eruption at 3600 14C years
Melanocratic nodule in Hbl–Pl andesite, 2005 eruption

Table 7. Representative analyses (wt %) of Cr-spinel inclusions in olivine from lavas of Young Shiveluch volcano

Component	Sample 7482			Sample 7487			Sample 7516-1			Sample 7499-4		
TiO_2	0.60	0.96	0.73	0.48	0.60	0.52	0.41	0.54	0.42	0.45	0.45	0.27
Al_2O_3	10.19	12.01	11.41	15.12	12.76	13.23	15.13	12.97	14.02	10.68	14.75	15.03
Cr_2O_3	48.72	41.98	46.08	45.31	44.88	44.39	44.29	37.99	39.57	45.18	46.53	49.92
FeO	9.62	13.17	8.04	8.02	10.88	10.53	9.46	16.3	14.37	12.90	7.66	5.26
Fe_2O_3	21.25	21.53	21.81	18.92	19.36	20.12	18.48	21.54	20.95	18.73	17.9	16.07
MnO	0.25	0.26	0.25	0.18	0.20	0.24	0.20	0.24	0.25	0.30	0.20	0.13
MgO	7.96	8.03	8.45	9.87	9.38	8.85	10.15	7.78	8.28	9.30	10.48	11.79
NiO	0.05	0.06	0.07	0.14	0.16	0.13	0.12	0.13	0.12	0.06	0.10	0.13
Total	98.66	98.07	97.84	98.1	98.27	98.07	98.32	97.58	98.05	97.66	98.13	98.68
Cr#	76.23	70.10	73.04	66.78	70.23	69.24	66.26	66.27	65.44	73.94	67.91	69.02
Mg#	34.52	32.27	36.55	42.79	38.92	37.2	42.69	29.86	32.62	37.77	45.57	52.89
Fo, mol %	88.41	86.09	87.28	88.62	87.79	89.30	89.14	86.91	86.91	91.23	90.40	91.96

Note: Fe_2O_3 and FeO concentrations are calculated from stoichiometric considerations, Cr# = 100Cr/(Cr + Al), Mg# = 100Mg/(Mg + Fe), *Fo* is the composition of the host olivine.

differentiation, and this predominantly controlled the composition of the evolving magmas.

The high ("adakitic") Sr/Y ratio of 30–71 and low Y concentrations of <18 ppm are typical of andesites of Young Shiveluch (Fig. 16). These features are often interpreted as testifying that melts derived from the subducted slab (eclogite) contributed to the composition of the magmas (see, for example, Yogodzinski et al., 2001; Churikova et al., 2001). Critically analyzing this hypothesis, we have to comment that the rock compositions of Young Shiveluch plot within the transition area between typical arc magmas (Sr/Y < 40; Defant and Drummond, 1990) and rocks with pronounced "adakitic" specifics (Sr/Y > 100, La/Yb > 20), such as magnesian andesites dredged from the western flank of the Komandorsky block (Yogodzinski et al., 1995) or andesites of Cook Island, Chile (Stern and Kilian, 1996). As was recently discussed in the literature, eclogite melting (in a subducted slab or in the lower crust) is not the only possible explanation of the genesis of rocks of composition transitional to adakite. Rocks with moderately high Sr/Y ratios can be generated by the crustal differentiation of magmas with low initial Sr/Y ratios, as is typical of arc magmas (see, for example, Richards and Kerrich, 2007; Moyen, 2009).

The rocks of Young Shiveluch volcano have a Sr/Y ratio positively correlated with the SiO_2 concentration (Fig. 16). The highest Sr/Y ratios are typical of the most evolved varieties, which have the highest Sr and lowest Y concentrations. As was discussed above, high Sr concentrations of differentiated rocks can be explained by the incomplete separation of plagioclase phenocrysts from the melt during magma fractionation. The Y concentrations of the rocks remain roughly the same within the range of 53–59 wt % SiO_2 and drastically decrease in more evolved rocks. Among the main mineral phases of the Young Shiveluch lavas, the most appreciable control on the Y and HREE concentrations of the rocks was exerted by amphibole, whose partition coefficients of these elements are equal to or greater than one (Brophy, 2008). As is demonstrated by the simulation of various scenarios for the partial melting of crustal rocks and magma crystallization at various depths (Brophy, 2008), this behavior of Y at increasing SiO_2 concentration is compatible with magma fractionation with the participation of amphibole in the upper or middle crust. The coupled effect of amphibole crystallization and the incomplete plagioclase separation from the crystallizing magma can explain the monotonous increase in the Sr/Y ratio in the Young Shiveluch rocks with an increase in their SiO_2 concentration without invoking any exotic models for the melting of the subducted slab under the volcano.

Role of Magma Mixing

A hybrid genesis of rocks is usually identified based on the occurrence of melanocratic nodules, unequilibrated mineral associations, corroded phenocrysts, and significant variations in the zoning of phenocrysts (see, for example, Eichelberger, 1978, 1980). A direct

Fig. 11. (a, b) Composition of the cores of olivine phenocrysts in rocks from Young Shiveluch volcano; variations in the concentrations of (c) CaO, (d) MnO, and (e) NiO in olivine from various ptgc rock types. The solid line in Fig. 11e shows the fractional crystallization trend, and the dashed line in the same figure shows the mixing trend of a primitive and an evolved melt.

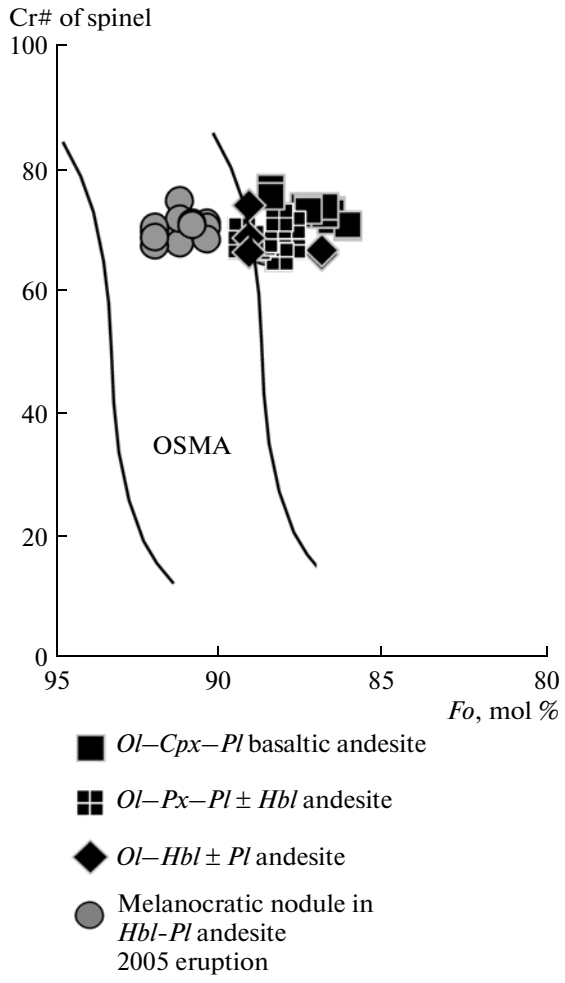

Fig. 12. Composition of spinel inclusions in olivine phenocrysts in lavas of Young Shiveluch volcano. OSMA is the field of the olivine–spinel assemblage in mantle rocks (Arai, 1994).

line of evidence in favor of mixing is the simultaneous eruption of magmas of different composition in the form of heterotaxitic lavas (Volynets, 1979). Traces of mixing of melts of different composition were described in Kamchatka for rocks erupted in 1996 in the Akademii Nauk caldera (Grib, 1997) and lavas of the volcanoes of Kizimen (Melekestsev et al., 1992; Trusov and Plechov, 2005; Churikova et al., 2007), Dikii Greben' (Bindeman, 1993), Malyi Smyachik (Leonov and Grib, 2004), Aag and Arik (Fedorov, 1972), and Ksudach (Volynets et al., 1999).

It was mentioned in (Volynets, 1979) that heterotaxitic pumice is contained in the pyroclastic deposits of Young Shiveluch volcano. Evidence of the interactions of compositionally contrasting melts was documented in the modern lavas of the volcano (Humphreys et al., 2006; Dirksen et al., 2006; Gorbach, 2006). It was also demonstrated above that magma mixing is a widespread process throughout the whole Holocene history of the volcano. This follows from the occurrence of heterotaxitic lavas, sharp (and often reversed) zoning of phenocryst minerals, and certain geochemical features of the rocks.

Plagioclase in Young Shiveluch rocks displays normal, reversed, and oscillatory types of its zoning, which is often discontinuous and involves drastic changes in the concentration of the anorthite end member (Fig. 5). For example, lavas of the 2004 eruption contain plagioclase phenocrysts whose cores define discrete groups of composition ranging from An_{32} to $An_{83–78}$ (Gorbach, 2006). In plagioclase phenocrysts with reversed zoning, the concentration of the anorthite end member drastically increases (by 25–29 mol %) at the boundary between the core and outer zone. The cores look like fused and resorbed. Plagioclase grains with patchy cores $An_{83–78}$ are overgrown by unzoned andesine $An_{47–49}$. These significant changes in the composition of zones could hardly be induced by minor pressure fluctuations in the magmatic chamber due to the uneven magma discharge during eruptions (Humphreys et al., 2006) or a temperature increase because of the release of the latent crystallization heat (Blundy et al., 2006). We believe that this sharp zoning should have been produced under the effect of significant changes in the physicochemical parameters of crystallization, perhaps, because of interaction of magmas of contrasting composition and temperature.

It was probably the mixing of contrasting magmas that resulted in the broad variations in the Al_2O_3 concentration (6–14 wt %) in hornblende crystals from the *Hbl–Pl* andesites (Fig. 8). High Al_2O_3 concentrations were detected in the marginal zones of phenocrysts in the lavas of the modern dome (Gorbach, 2006), in amphiboles in the heterotaxitic lavas, and at the contacts of a melanocratic nodule with its host andesite. For example, needle-shaped amphibole in the nodule contains 10–13 wt % Al_2O_3, while hornblende in the host andesite contains 7–9 wt % Al_2O_3. Zonal crystals with an aluminous outermost zone grew along the contact of the nodule and lava. This setting of the phenocrysts testifies that temperature played a decisive role in the growth of the aluminous outer zones of amphibole in the *Hbl–Pl* andesites. This conclusion is consistent with experimental data (see, for example, Scailett and Evans, 1999), which indicate that Al_2O_3, Na_2O, and TiO_2 concentrations of amphibole increase with increasing temperature. It is also worth mentioning that hornblende in rocks of Young Shiveluch volcano is extensively opacitized, with obvious indications of mixing of magmas of contrasting composition (*Ol–Px–Pl ± Hbl* andesites). As was demonstrated in (Plechov et al., 2007), this suggests that hornblende decomposed at increasing temperature during the mixing of evolved and primitive magmas.

Magma mixing also affected the composition of minerals during earlier crystallization stages. As can be seen in Fig. 11, the fractional crystallization of olivine in a basaltic melt should have rapidly depleted Ni in the melt

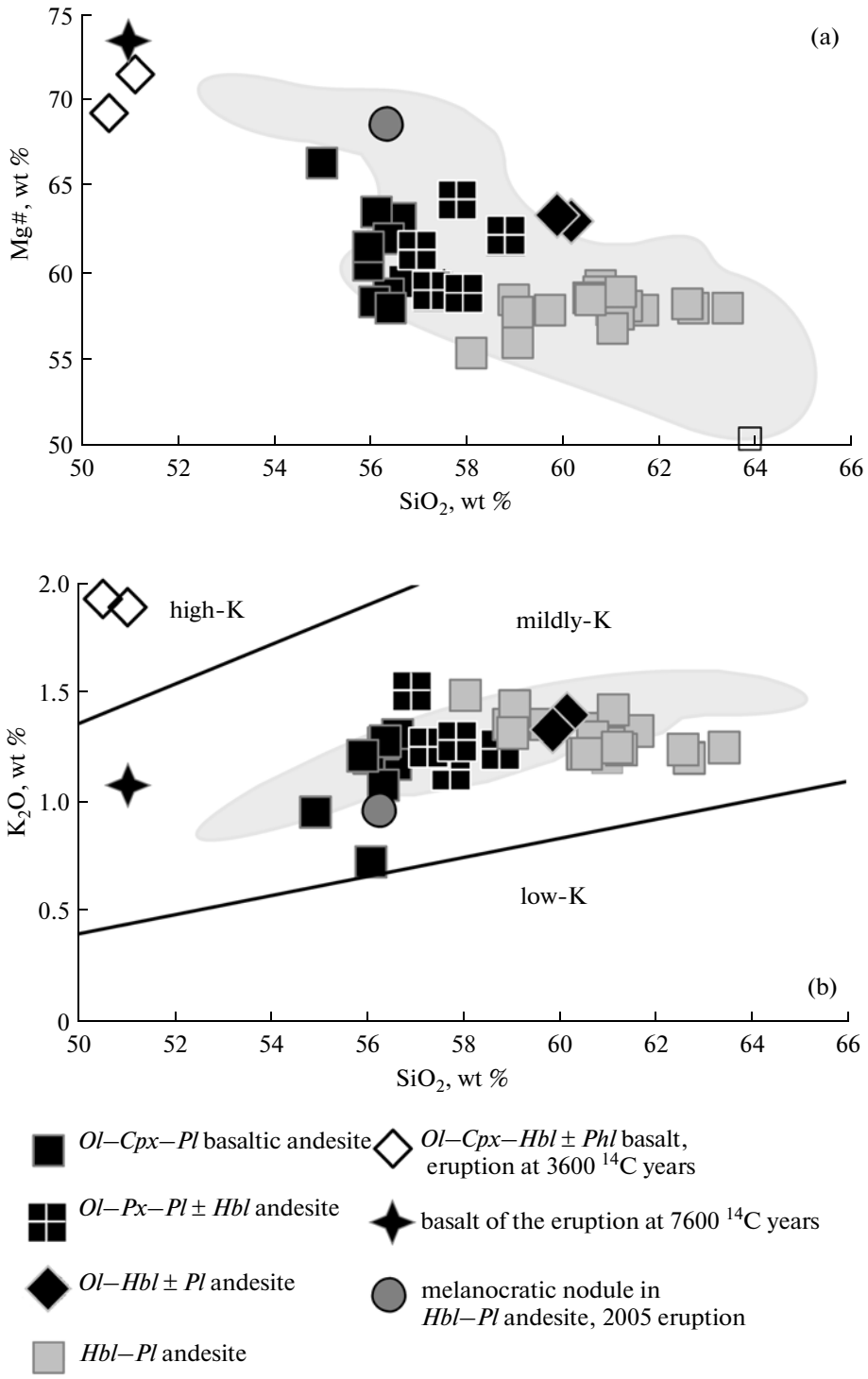

Fig. 13. Composition of rocks in the lava complex of Young Shiveluch volcano in (a) SiO_2–Mg# and (b) SiO_2–K_2O diagrams. The composition of basalts of the eruption at 7600 ^{14}C years is according to (Volynets et al., 1997). The gray field shows the composition of proximal pyroclastic deposits of Young Shiveluch volcano (Ponomareva et al., 2007).

and, consequently, in the equilibrium olivine. If a primitive and evolved melts mix, the hybrid magma bears a higher Ni concentration, at the same Mg#, than the differentiation products of basalts. Olivine crystallizing from such hybrid magma should also have elevated Ni concentrations. Deviations of olivine compositions in the *Ol–Px–Pl* ± *Hbl* andesites toward higher NiO concentrations at approximately the same forsterite con-

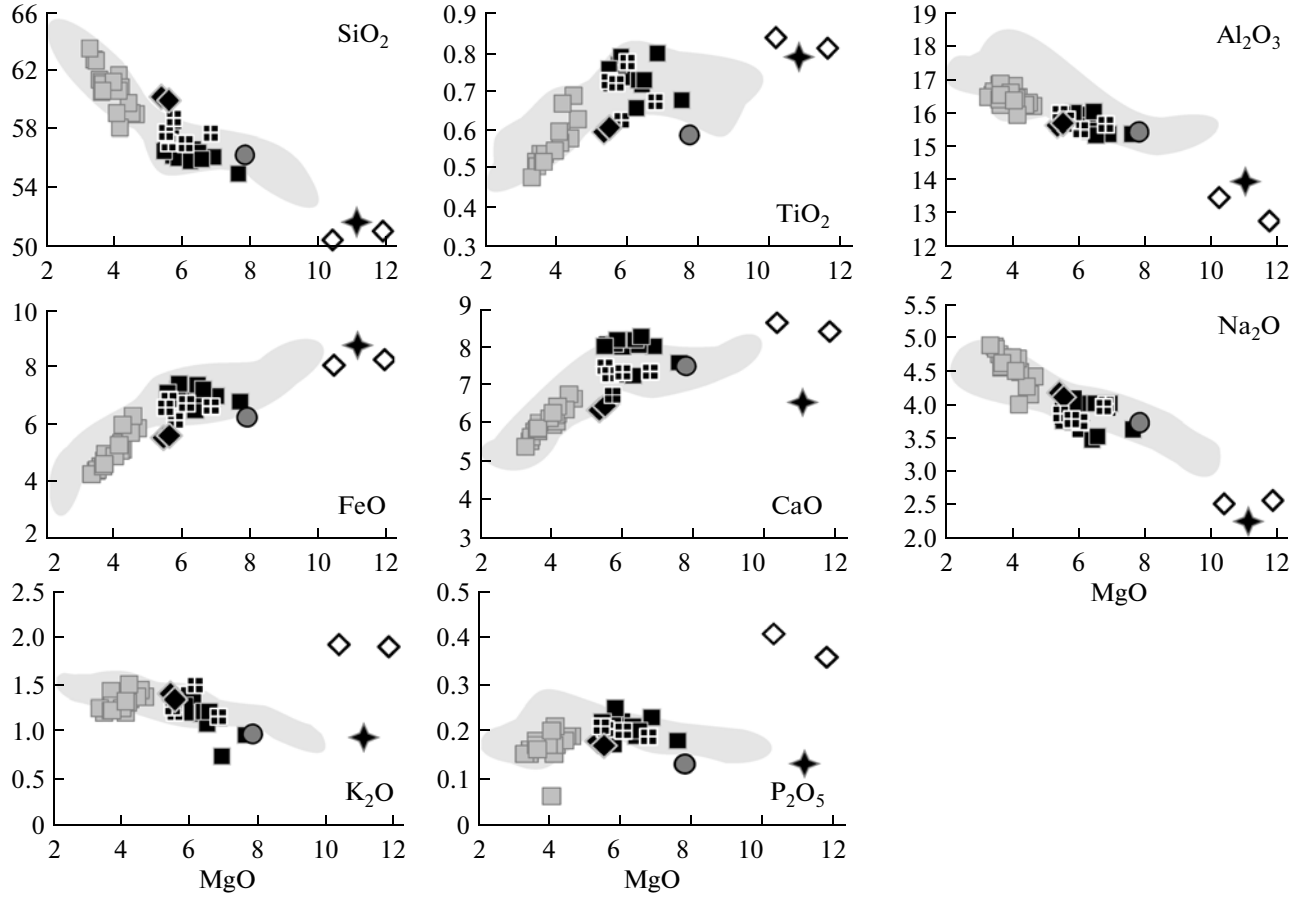

Fig. 14. Variations in the concentrations of major oxides vs. MgO in rocks from Young Shiveluch volcano. See Fig. 13 for symbol explanations.

centration in the olivine as in olivine in the melanocratic nodule and *Ol–Cpx–Hbl* ± *Phl* basalts can be explained by the hybrid nature of these rocks, which were produced by the mixing of primitive basalts and differentiated andesites.

Magma mixing most significantly affected the Cr and Ni concentrations, which are the most contrasting in the primitive and evolved rocks. In the Cr vs. SiO_2 plot (Fig. 17), the trend predicted for the fractional crystallization of basaltic melt has a hyperbolic configuration and leads to a significant depletion of the melts in Cr (as well as Ni) during early crystallization stages. The data points of lavas from Young Shiveluch plot away from the crystallization trend and define diffuse linear trends, which suggests that these magmas were produced by the mixing of primitive basalt magma and variably evolved andesites. This process can account for the elevated Cr and Ni concentrations of the andesites in the Young Shiveluch andesites, which is an identification feature of the Holocene tephra of this volcano and makes this volcano different from other ones in Kamchatka (Ponomareva et al., 2007).

The mixing of primitive and evolved magmas can explain the origin of the magnesian andesites of Young Shiveluch volcano but cannot answer the question as to why magnesian andesites occur only at Young Shiveluch of all volcanoes in Kamchatka, in spite of the fact that mixing processes are widespread in all of the volcanic zones (Volynets, 1979; Grib, 1997; Melekestsev, 1992; Trusov and Plechov, 2005; Churikova et al., 2007; Bindeman, 1993; Leonov and Grib, 2004, Fedotov, 1972; Volynets et al., 1999; Eichelberger and Izbekov, 2000). A possible explanation of this phenomenon is the significant difference between the most primitive magmas of volcanoes in the Central Kamchatkan Depression and in the Eastern Volcanic Front. The primitive basalts and basaltic andesites reaching the surface at Shiveluch and of the volcanoes of the Central Kamchatkan Depression have high Mg# > 0.65 and high concentrations of Ni (>100 ppm) and Cr (>500 ppm), which are close to those in the probable mantle magmas (see, for example, Portnyagin et al., 2007). The most primitive rocks of the Eastern Volcanic Front usually have a differentiated high-Al composition (Mg# < 0.6, Ni < 50 ppm, Cr < 150 ppm) (*Geochemical Types...*, 1990). Obviously, the emplacement of these basalts at upper crustal levels was predated by deep differentiation, and their mixing with

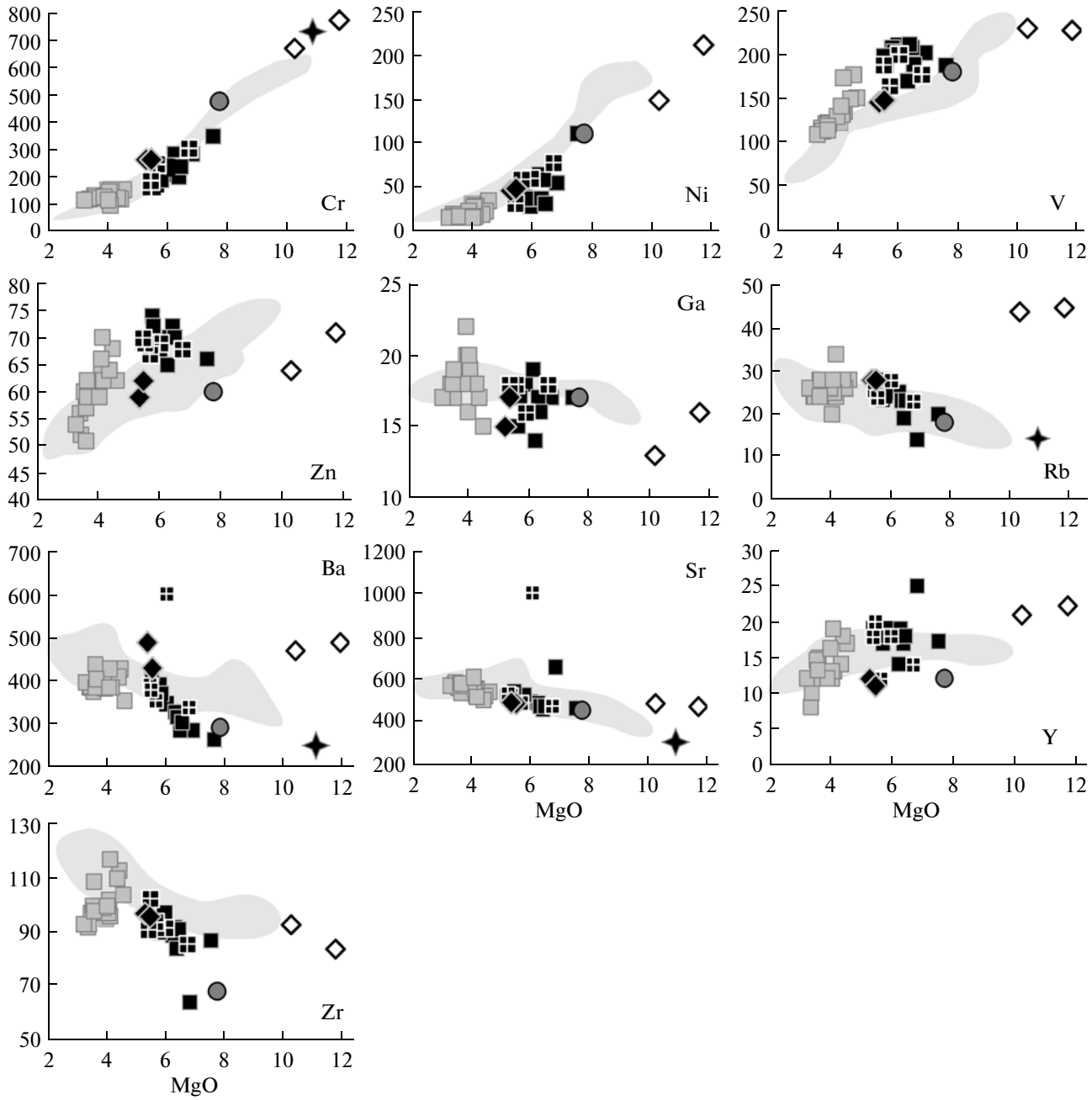

Fig. 15. Variations in the concentrations of trace elements vs. MgO in rocks from Young Shiveluch volcano. See Fig. 13 for symbol explanations.

silicic magmas could not generate melts of composition comparable with that of magnesian andesites of Young Shiveluch volcano (Fig. 17).

Our conclusion about the hybrid nature of the magnesian andesites at Young Shiveluch does not rule out the possibility that andesites magmas of mantle provenance could be involved in magmatic processes in Kamchatka. Aphyric, in contrast to Shiveluch andesites, primitive andesite (58.4 wt % SiO_2, Mg# = 0.70) was documented in the Shisheiskii volcanic complex (Portnyagin et al., 2007). Although we cannot rule out that magmas of this composition could contribute to the origin of the Young Shiveluch rock series, it seems to be more probable that the parental magmas had a basalt–basaltic andesite composition with ≤54 wt % SiO_2 (Portnyagin et al., 2007; Portnyagin and Manea, 2008).

The anomalous enrichment of Sr and Ba in the Mount Karan extrusion and elevated K, P, Rb, Ba, and Sr concentrations in the *Ol–Cpx–Hbl* ± *Phl* basalts cannot be explained by the crystallization differentiation of the Young Shiveluch magmas or their mixing. A possible explanation for the anomalous composition

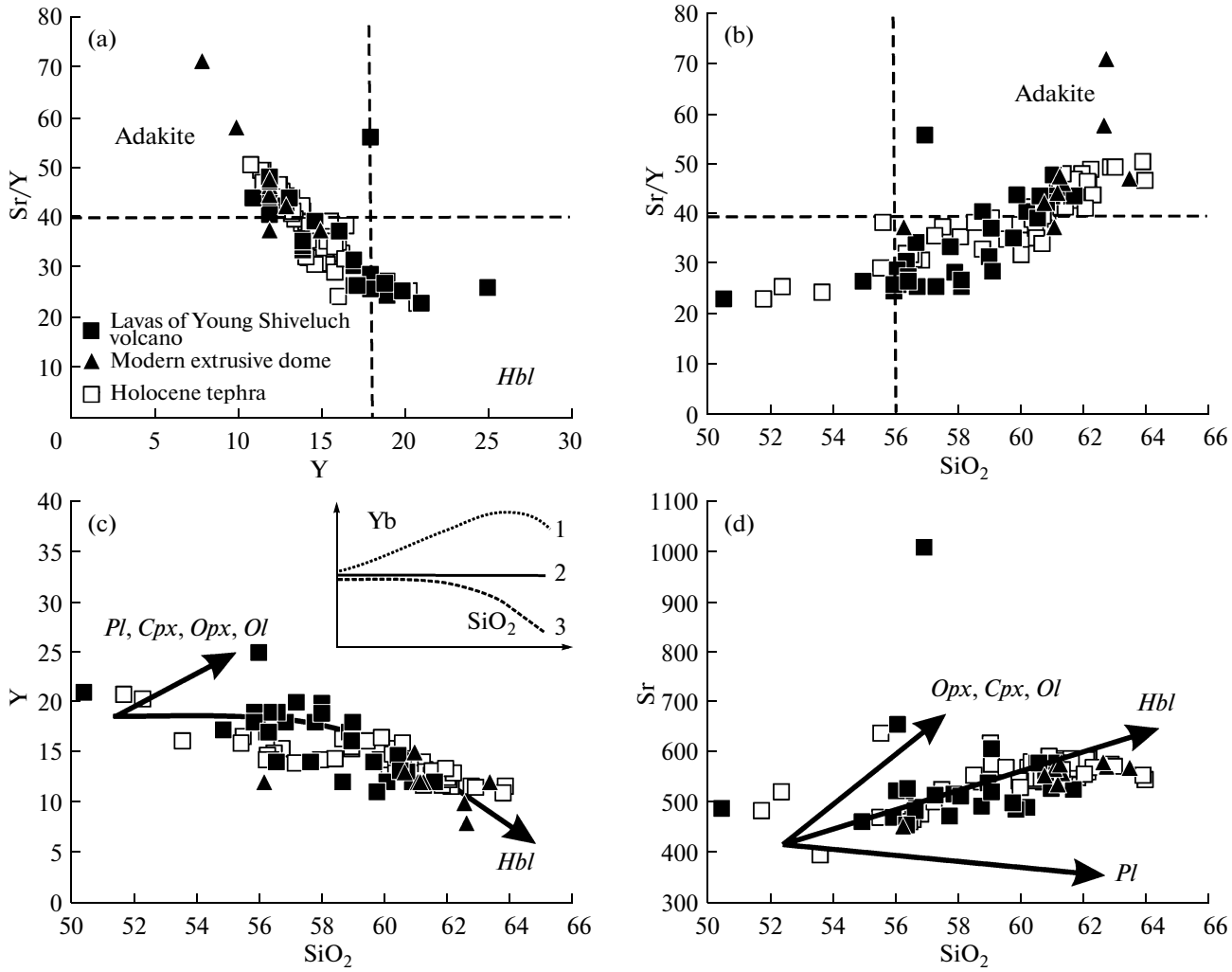

Fig. 16. Variations in the concentrations of SiO_2, Sr, and Y in lavas and pyroclastic rocks of Young Shiveluch volcano. Lava compositions are our data, compositions of pyroclastic rocks are according to (Ponomareva et al., 2007). The field of adakite compositions (Y < 18 ppm, Sr/Y > 40, SiO_2 > 56 wt %) is shown according to (Defant and Drummond, 1990). The inset in Fig. 16c shows trends for Yb (a close geochemical analogue of Y) in the crystallization course of basalt melt (1) without and (2) with amphibole under lower crustal conditions and (3) a trend based on data in (Brophy, 2008). The heavy arrows in Figs. 16c and 16d show the vectors of the melt compositional evolution during the crystallization of various phases.

of the lavas of Mount Karan is the contamination of the andesite magmas with crustal rocks, for example, silty marl, such as exposed near the northern slope of the extrusion (Fig. 3b). To explain the enrichment of the primitive *Ol–Cpx–Hbl ± Phl* basalts in certain incompatible trace elements, it was suggested (Portnyagin et al., 2007) that metasomatized mantle material could be involved in magma generation.

Conditions of Magma Evolution

The petrography and mineralogy of rock of the lava complex at Young Shiveluch provide a record of various stages of magma fractionation and hybridism. The character of variations in the contents of major oxides and trace elements in the rocks suggest that the mixed magmas were variably differentiated. This conclusion finds support in field relations: flows of the heterotaxitic lavas provide evidence of the incomplete mixing of *Ol–Cpx–Pl* basaltic andesite and *Hbl–Pl* andesite. These melts were simultaneously brought to the surface and, hence, should have coexisted in the feeding system of the volcano. To explain this fact, it should be assumed that the feeding system of Young Shiveluch was zonal in terms of composition and temperature and can be visualized as either a single large layered chamber or a number of chambers that occurred at various depths and were filled with variably evolved magmas.

Data on the chemistries of minerals more favor the existence of two or more magmatic chambers at various depths. The hornblende andesites of the modern eruptions crystallized in shallow-depth magmatic chambers. The temperature of the andesites before the

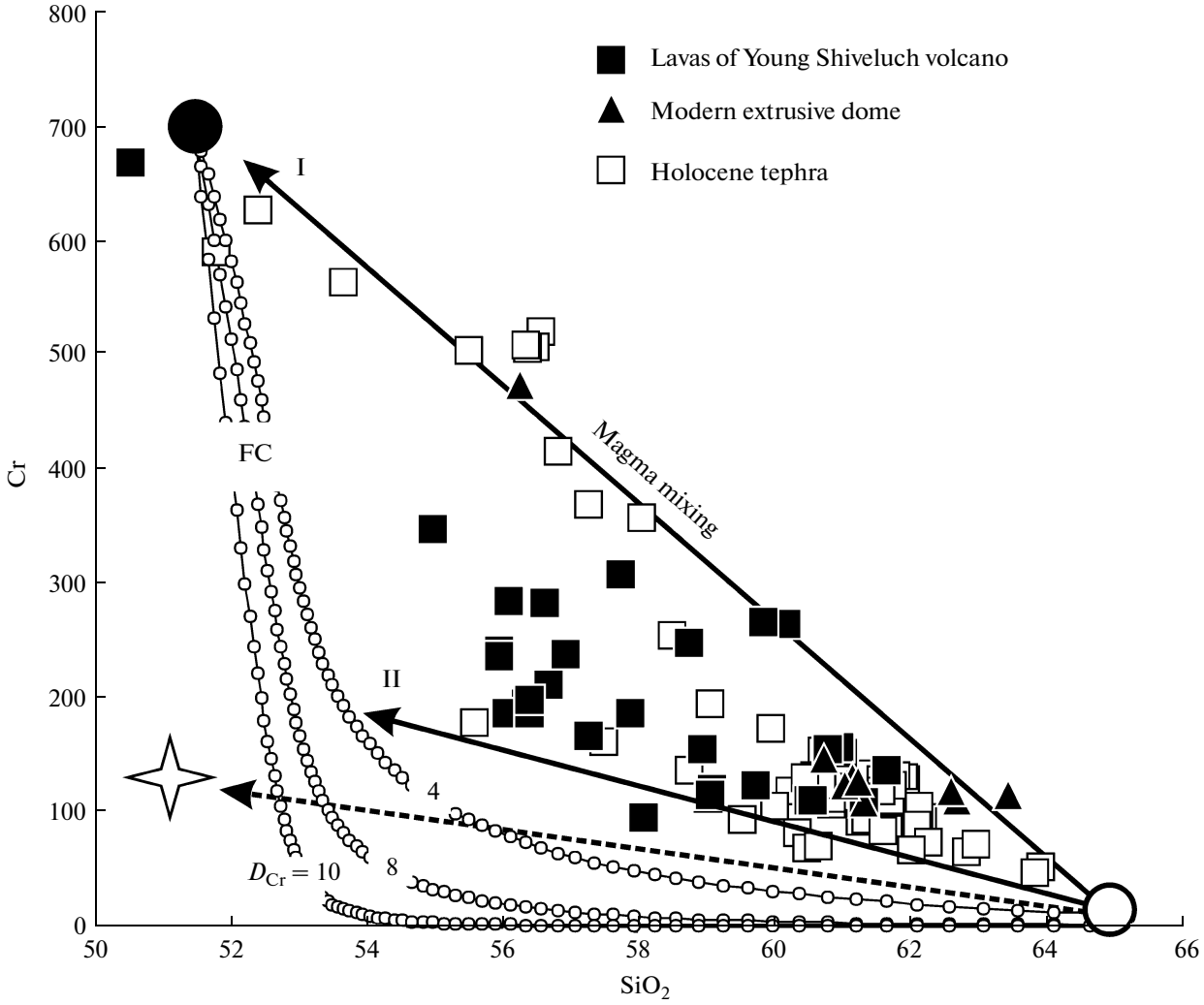

Fig. 17. Variations in the concentrations of SiO_2 and Cr in lavas and pyroclastic rocks of Young Shiveluch volcano. Lava compositions are our data, compositions of pyroclastic rocks are according to (Ponomareva et al., 2007). Thin lines with circles show the model trends of fractional crystallization FC of basalt melt with initial concentrations of Cr = 700 ppm and SiO_2 = 51.5 wt % (solid circle) at various values of the bulk partition coefficient D_{Cr} between minerals and melt. The calculations were made using the dependence between the SiO_2 concentration and degree of crystallization, according to (Brophy, 2008). Heavy arrows show possible mixing trends of a differentiated magma with 65 wt % SiO_2 (open circle) and (I) primitive basalt, and (II) basaltic andesite obtained by 35% crystallization of primitive melt. The dashed line with an arrowhead shows the mixing trend of differentiated andesite and an average composition of high-Al basalt of the mildly-K series (star) of the Eastern Volcanic Front (*Geochemical Types...*, 1990).

2001 eruption was estimated at approximately 840°C at an oxygen fugacity of 1.5–2.1 log units above the NNO buffer (from +2.1 to +2.7 QFM) (Humphreys et al., 2006). The maximum pressure of about 1.6 kbar calculated for the maximum H_2O content (5.1 wt %) in melt inclusions from the *Hbl–Pl* andesite suggests that the magmatic chamber could occur at a depth of 5–6 km below the summit of the volcano (Humphreys et al., 2006). Similar conclusions were drawn in (Zharinov and Demyanchuk, 2008) from data on the volume and discharge of lavas that form the modern extrusive dome.

The mineralogy of the olivine–clinopyroxene–plagioclase basaltic andesites and olivine–hornblende plagioclase-bearing andesites suggests that these rocks should have crystallized at greater depths. A high pressure during the crystallization of pargasite amphibole in the *Ol–Hbl ± Pl* andesites follows from the occurrence of this amphibole in association with magnesian olivine. It was demonstrated in (Grove et al., 2003) that this association can be produced by the crystallization of water-rich basalt melts under a high pressure. For instance, pargasitic hornblende occurring in lavas of Mount Shasta volcano as rims around magnesian olivine and pyroxene is analogous to amphibole experimentally obtained from water-rich magnesian basalt under a pressure of 8 kbar (Grove et al., 2003). According to the empirical geothermometer (Anderson and Smith, 1995), the pressure during the crystallization of

highly aluminous (Al_{tot} = 2–2.6 f.u.) amphibole of the *Ol–Hbl ± Pl* and *Ol–Px–Pl ± Hbl* andesites of Young Shiveluch was approximately 7–9 kbar. The oxygen fugacity, which was calculated using the assemblage of olivine and Cr-spinel (Ballhaus et al., 1991) for the *Ol–Hbl ± Pl* andesites, is 2.1 ± 0.38 log units higher than the QFM buffer. The oxygen fugacity of the *Ol–Cpx–Pl* basaltic andesite and *Ol–Px–Pl ± Hbl* andesites was slightly lower: +1.8 ± 0.15 and +1.7 ± 0.27 QFM, respectively. The temperature of the basaltic andesite lavas before their eruption was close to 1100°C, according to the graphical two-pyroxene geothermometer (Lindsley, 1983).

The simplest interaction scheme of two compositionally distinct magmas in the feeding system of the volcano is shown in Fig. 18. According to (Sparks et al., 1977), high-density and hot basaltoid magmas should have been concentrated at the bottom of a magmatic chamber filled with a mush of previously formed crystals in differentiated matrix melt (crystal mush) and should induce heating and convection at the high levels. The mafic melt should thereby become disseminated in the form of mafic globules and melanocratic nodules (Bindeman, 1993). Convection could bring cumulus material concentrated at chamber walls (which is fairly abundant in extrusive lavas) into the main volume of the chamber.

The dynamics and composition of the products of the 2001–2009 eruptions are in good agreement with this model. The beginning of the 2001 eruption was predated by intense seismicity in the lower crust. The inset in Fig. 18 shows the distribution of earthquake centers during the time period starting in January 2000 until October 2001 (data provided by the Kamchatka branch of the Geophysical Survey of the Russian Academy of Sceinces). An aseismic region can be distinguished at depths of approximately 12–22 km, and an intermediate chamber can occur within this region. The extrusive lavas erupted in 2001–2002, 2004 (Humphreys et al., 2006; Dirksen et al., 2006; Gorbach, 2006), 2005, and during the current eruption show traces of hybridism. The probable time when more mafic magmas were injected into the shallow-depth magmatic chamber was evaluated at 60–360 days before the 2001–2002 eruption (Dirksen et al., 2006). The variable composition of the extrusive lavas erupted in 2004–2008 (Table 1, samples 7433, 7452-1, 7452-7, 7515, 7515-1, and 7555) suggests that convection could proceed in the shallow-depth magmatic chamber.

Replenishment Periodicity of the Magmatic Chamber

The vertical section of the Holocene pyroclastic material consists of three units that have a mafic composition principally different from the composition of the monotonously predominant andesites (Ponomareva et al., 2007). This is tephra of mildly potassic basaltic andesite dated at 7600 ^{14}C years, highly potassic basalts of 3600 ^{14}C years, and basaltic andesites and lavas of contrasting composition (older than the eruption) dated at 3700 ^{14}C years. The compositional similarities between the material of the upper clastic unit at Site 7533 at the Sukhoi Il'chinets River and the rocks of the oldest extrusions and lava flows at Young Shiveluch suggest that the first episode of more mafic lava eruptions occurred earlier than 10000 ^{14}C years. It can be hypothesized that this time period was marked by the replenishment of the shallow-depth magmatic chamber beneath the volcano. If this was actually the case, the eruption products of the intermediate cycles should display a basic to acid compositional trend of the lava and pyroclastic material due to progress in magma fractionation with time. However, in fact, the composition of pyroclastic material produced during intermediate eruptions of Young Shiveluch does not any significantly vary but is rather uniform: 60–62 wt % SiO_2 and Mg# = 58–60 (Ponomareva et al., 2007). Only single eruptions produced more mafic rocks. For example, the pumices erupted in 1964 had taxitic varieties with individual bands and schlieren with 60–62 and 56 wt % SiO_2 (Ivanov, 2008), and the tephra erupted in 1854 has 55.6 and 57.5 wt % SiO_2 (Ponomareva et al., 2007). These compositional evolution of the eruption products with time is more consistent with small but frequent injections of basaltoid magmas at the lower levels of the magmatic chamber. The 3600–3700, 7600, and eruptions older than approximately 10000 ^{14}C years were likely related to more active replenishment of deep magma. As was demonstrated in (Volynets et al., 1997), the eruptions at 3600 and 7600 ^{14}C years were coeval with the regionally spread episode of volcanic activation in Kamchatka.

CONCLUSIONS

We obtained the first detailed geological and petrologic–geochemical data on the lava complex of Young Shiveluch volcano. These data led us to the following conclusions:

(1) The lava complex of Young Shiveluch volcano includes extrusive bodies, lava flows, and dikes of various composition and age. The volume of lavas in the modern edifice of Young Shiveluch is no greater than 25 km^3. Taking into account the material of the debris avalanches, the volume of the Young Shiveluch lavas and extrusions of the Karan group is close to 50 km^3, which corresponds to one-third of the total volume of magmas erupted by the volcano in the Holocene.

(2) The lavas of Young Shiveluch volcano are predominantly magnesian andesites of the mildly potassic calc–alkaline series that were produced by the fractional crystallization of a primitive melt and its mixing with silicic derivatives. The activity of Young Shiveluch is related to the periodic replenishment of primitive magmas in a shallow-depth chamber, which is filled with a mush of older crystals and residual melt.

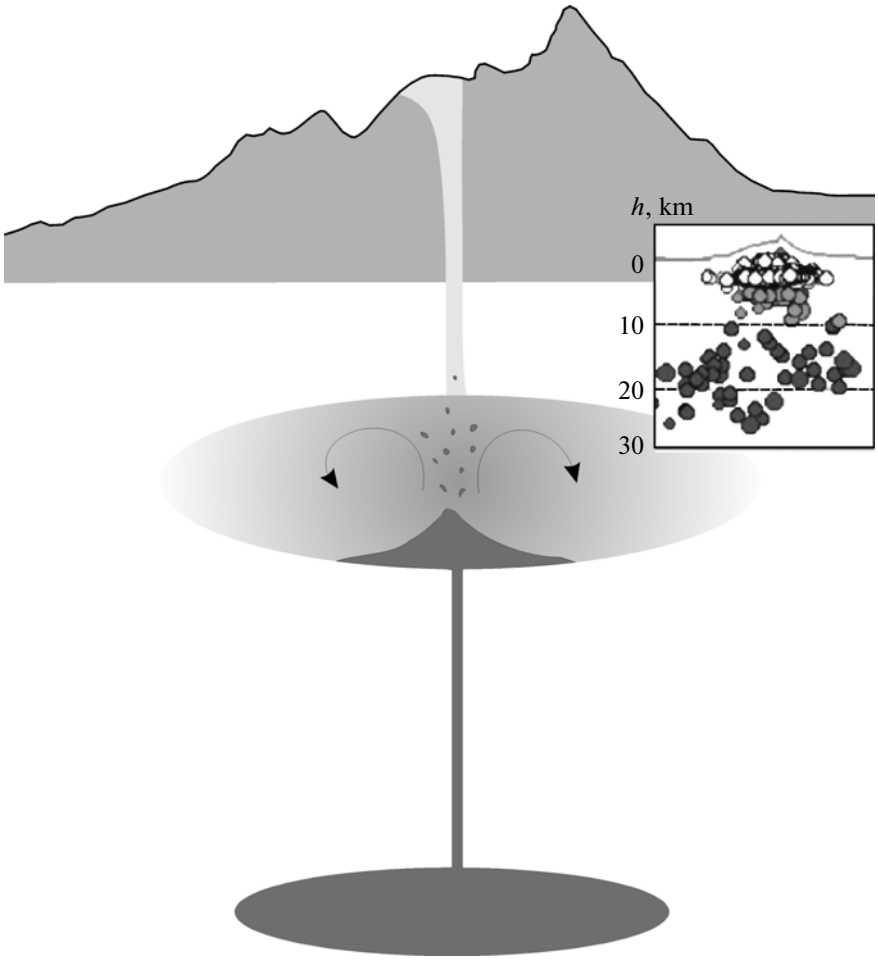

Fig. 18. Hypothetical model for the mixing of variably evolved melts in the magmatic feeding system of Young Shiveluch volcano. See text for explanations. The inset shows the distribution of volcanic earthquake centers during the time span starting in January 2000 until October 2001 (data of the Kamchatka Branch of the Geophysical Survey, Russian Academy of Sciences).

(3) Geological lines of evidence of the mixing processes are provided by lavas of heterotaxitic structure and by the occurrence of melanocratic nodules in the lavas of the modern extrusive dome. The mineralogical lines of evidence are compositionally discrete groups of hornblende and plagioclase phenocryst cores and their sharp zoning, the occurrence of highly magnesian olivine in all rock varieties, the reaction relations of this mineral with pyroxenes and hornblende, and the reversed zoning of the pyroxenes.

(4) The "adakitic" geochemical characteristics ($Sr/Y > 50$, $Y < 18$ ppm) of andesites of Young Shiveluch volcano are most clearly pronounced in the most evolved rock varieties and are produced by the fractional crystallization of an association of plagioclase and hornblende at the incomplete separation of plagioclase crystals from the fractionating magmas.

ACKNOWLEDGMENTS

The authors thank T.M. Filosofova (Institute of Volcanology and Seismology, Far East Branch, Russian Academy of Sciences), D. Rau, and M. Toener (IFM-GEOMAR) for help with the analytical work. M.M. Pevzner (Geological Institute, Russian Academy of Sciences) is thanked for dating the rocks. The authors highly appreciate the valuable comments expressed by V.V. Ponomareva (Institute of Volcanology and Seismology, Far East Branch, Russian Academy of Sciences) and A.A. Babanskii (Institute of the Geology of Ore Deposits, Petrography, Mineralogy, and Geochemistry, Russian Academy of Sciences) when discussing the manuscript. Special thanks are due the mountain-climber to R. Sagitova, S. Samoilenko and T. Manevich of the Laboratory of Active Volcanism and Eruption Dynamics (Institute of the Geology of Ore Deposits, Petrography, Mineralogy, and Geochemistry, Russian Academy of Sciences) for

organizing the fieldwork. The fieldwork was financially supported by Grants 06-III-V-08-369 and 07-III-D-08-094 of the Far East Branch, Russian Academy of Sciences; the analytical studies were carried out under the KALMAR Russian–German joint project (subproject "Spatial and Temporal Evolution of Volcanism and Magmatism in the Aleutians–Kamchatka Junction Zone"), which is financially supported by the Ministry of Science and Education of Germany.

REFERENCES

1. Arai, S., Compositional Variation of Olivine–Chromian Spinel in Mg-Rich Magmas as a Guide to Their Residual Spinel Peridotite, *J. Volcanol. Geotherm. Res.*, 1994, vol. 114, pp. 279–293.
2. Anderson, J.L. and Smith, D.R., The Effects of Temperature and f_{O_2} on the Al-in-Hornblende Barometer, *Am. Mineral.*, 1995, vol. 80, pp. 549–559.
3. Ballhaus, C., Berry, R., and Green, D., High-Pressure Experimental Calibration of the Olivine–Orthopyroxene–Spinel Oxygen Geobarometer Implications for the Oxidation State of the Upper Mantle, *Contrib. Mineral. Petrol.*, 1991, vol. 107, pp. 27–40.
4. Bindeman, I.N., Retrograde Vesicular Basaltic Magmas in the Shallow Chambers: The Model for Origin of Melanocratic Inclusions in the Felsic and Intermediate Rocks, *Petrologiya*, 1993, vol. 6, no. 2, pp. 632–644.
5. Blundy, J., Cashman, K., and Humphreys, M., Magma Heating by Decompression-Driven Crystallization Beneath Andesite Volcanoes, *Nature*, 2006, vol. 443, pp. 76–80.
6. Brophy, J.G., A Study of Rare Earth Element (REE)–SiO_2 Variations in Felsic Liquids Generated by Basalt Fractionation and Amphibolite Melting: a Potential Test for Discriminating between the Two Different Processes, *Contrib. Mineral. Petrol.*, 2008, vol. 156, pp. 337–357.
7. Churikova, T., Dorendorf, F., and Wörner, G., Sources and Fluids in the Mantle Wedge below Kamchatka, Evidence from Across-Arc Geochemical Variation, *J. Petrol.*, 2001, vol. 42, pp. 567– 593.
8. Churikova, T., Worner, G., Eichelberger, J., and Ivanov, B., Minor- and Trace Element Zoning in Plagioclase from Kizimen Volcano, Kamchatka: Insights on the Magma Chamber Processes, in *Volcanism and Tectonics of the Kamchatka Peninsula and Adjacent Arcs*, Eichelberger, J., Gordeev, E., Kasahara, M., Izbekov P., and Lees, J. Eds., *Geophys. Monogr. Ser.*, 2007, vol. 172, pp. 303–324.
9. Defant, M.J. and Drummond, M.S., Derivation of Some Modern Arc Magmas by Melting of Young Subducted Lithosphere, *Nature*, 1990, vol. 347, pp. 662–665.
10. Dirksen, O., Humphreys, M.C.S., Pletchov, P., et al., The 2001–2004 Dome-Forming Eruption of Shiveluch Volcano, Kamchatka: Observation, Petrological Investigation and Numerical Modelling, *J. Volcanol. Geotherm. Res.*, 2006, no. 155, pp. 201–226.
11. Dvigalo, V.N., Dome Growth in a Crater of Shiveluch Volcano in 1980–1981 Based on Photogrammetric Data, *Vulkanol. Seismol.*, 1984, no. 2, pp. 104–109.
12. Eichelberger, J.C. and Izbekov, P.E., Eruption of Andesite Triggered by Dike Injection: Contrasting Cases at Karymsky Volcano, Kamchatka and Mount Katmai, Alaska, *Philos. Trans., R. Soc., Mathem., Phys., and Eng. Sci.*, 2000, vol. 358, no. 1770, pp. 1465–1485.
13. Eichelberger, J.C., Andesitic Volcanism and Crustal Evolution, *Nature*, 1978, vol. 275, pp. 21–27.
14. Eichelberger, J.C., Vesiculation of Mafic Magma During Replenishment of Silicic Magma Reservoirs, *Nature*, 1980, vol. 288 P, pp. 446–450.
15. Fedorov, M.V., On Heterogeneity of Magmatic Melt of Aag-Arik Volcanoes, *Byull. Vulkanol. St.*, 1972, no. 48, pp. 48–50.
16. Fedotov, S.A., Dvigalo, V.N., Zharinov, N.A., et al., Eruption of Shiveluch Volcano in May–July, 2001 *Vulkanol. Seismol.*, 2001, no. 6, pp. 1–13.
17. *Geokhimicheskaya tipizatsiya magmaticheskikh i metamorficheskikh porod Kamchatki* (Geochemical Types of the Magmatic and Metamorphic Rocks in Kamchatka), Krivenko, A.P., Ed., *Tr. Inst. Geol. Geofiz. Sib. Otd. Akad. Nauk SSSR*, 1990, vol. 390.
18. Gorbach, N.V., New lava of Shiveluch volcano: evidence of magma mingling? In *Proceedings of 5th Biennial Workshop on Subduction Process Emphasizing the Japan–Kurile–Kamchatka–Aleutian Arcs (JJKASP-5), Japan, 2006,* 2006, pp. 133–137.
19. Gorbach, N.V., First Lava Flow on the Extrusive Dome of Shiveluch Volcano, 2004, *Vulkanol. Seismol.*, 2006, no. 2, pp. 9–16.
20. Gorshkov, G.S. and Dubik, Yu.M., Directed Explosion of Shiveluch Volcano, in *Vulkany i izverzheniya* (Volcanoes and Eruptions), Moscow: Nauka, 1969, pp. 3–38.
21. Grib, E.N., Petrology of Volcanic Products of 2–3 January 1996 Eruption in the Akademii Nauk Caldera, *Vulkanol. Seismol.*, 1997, no. 5, pp. 71–97.
22. Grove, T.L., Elkins-Tanton, L.T., Parman, S.W., et al., Fractional Crystallisation and Mantle-Melting Controls on Calc-Alkaline Differentiation Trends, *Contrib. Mineral. Petrol.*, 2003, no. 145, pp. 515–533.
23. Humphreys, M.C.S., Blundy, J.D., and Sparks, R.S.J., Magma Evolution and Open-System Processes at Shiveluch Volcano: Insights from Phenocryst Zoning, *J. Petrol.*, 2006, vol. 47, no. 12, pp. 2303–2334.
24. Humphreys, M.C.S., Blundy, J.D., and Sparks, R.S.J., Shallow-Level Decompression Crystallisation and Deep Magma Supply at Shiveluch Volcano, *Contrib. Mineral. Petrol.*, 2008, vol. 155, no. 1, pp. 45–61.
25. Ivanov, B.V., *Andezity Kamchatki (Spravochnik khimicheskikh analizov vulkanitov i osnovnykh porodoobrazuyushchikh mineralov)* (Andesites of Kamchatka: Chemical Analyses of Volcanic Rocks and Major Rock-Forming Minerals), Moscow: Nauka, 2008.
26. Jarosevich, E.J., Nelen, J.A., and Norberg, J.A., Reference Sample for Electron Microprobe Analysis, *Geost. Newslett.*, 1980, vol. 4, pp. 43–47.
27. Khubunaya, S.A., Bogoyavlenskii, S.O., Novgorodtseva, T.Yu., and Okrugina, A.I., Mineralogical Features of Magnesian Basalts as Reflection of Fractionation in the Magmatic Chamber of Klyuchevskoi Volcano, *Vulkanol. Seismol.*, 1993, no. 3, pp. 46–68.

28. Khubunaya, S.A., Zharinov, N.A., Murav'ev, Ya.D., et al., Eruption of Shiveluch Volcano in 1993, *Vulkanol. Seismol.*, 1995, no. 1, pp. 3–20.

29. Leonov, V.L. and Grib, E.N., *Strukturnye pozitsii i vulkanizm chetvertichnykh kal'der Kamchatki* (Structural Position and Volcanism of the Quaternary Calderas in Kamchatka), Vladivostok: Dal'nauka, 2004.

30. Lindsley, D.H., Pyroxene Thermometry, *Am. Mineral.*, 1983, vol. 68, pp. 477–493.

31. Lopatin, V.B., Litvinov, A.F., Tsikunov, A.G., et al., Geologicheskoe stroenie i poleznye iskopaemye ploshchadi listov O-57-XXV, XXXVI (Otchet o geologicheskoi s"emke i poiskakh poleznykh iskopaemykh M-Ba 1 : 200000, provedennykh Shiveluchskoi Partiei) (Geological Structure and Mineral Resources of the Area of Map Sheets O-57-XXV, XXXVI (Report on Geological Survey and Search for Mineral Resources on 1 : 200000 Scale Conducted by the Shiveluch Party in 1976–1978)) 3 vols., 1979.

32. Melekestsev, I.V., Dvigalo, V.N., Kirsanova, T.P., et al., 300 Years of Activity of the Kamchatka Volcanoes: Young Shiveluch (Analysis of Dynamics and Consequences of Eruptive Activity in 17–20 Centuries) Part 1. 1650–1964, *Vulkanol. Seismol.*, 2003, no. 5, pp. 3–19.

33. Melekestsev, I.V., Dvigalo, V.N., Kirsanova, T.P., et al., 300 Years of Activity of the Kamchatka Volcanoes: Young Shiveluch (Analysis of Dynamics and Consequences of Eruptive Activity in 17–20 Centuries) Part 2. 1965–2000, *Vulkanol. Seismol.*, 2004, no. 1, pp. 3–20.

34. Melekestsev, I.V., Ponomareva, V.V., and Volynets, O.N., Kizimen Volcano (Kamchatka)—A Future St.-Helens?, *Vulkanol. Seismol.*, 1992, no. 4, pp. 3–32.

35. Melekestsev, I.V., Volynets, O.N., and Ermakov, V.A.,et al., Shiveluch Volcano, in *Deistvuyushchie vulkany Kamchatki* (Active Volcanoes in Kamchatka), Moscow: Nauka, 1991, vol. 1, pp. 84–103.

36. Menyailov, A.A., Shiveluch Volcano: Its Geological Structure, Composition, and Eruptions, *Tr. Lab. Vulkanologii AN SSSR,* 1955, no. 9, p. 264.

37. Münker, C., Wörner, G., Yogodzinski, G.M., and Churikova, T., Behavior of High Field Strength Elements in Subduction Zones: Constraints from Kamchatka–Aleutian Arc Lavas, *Earth Planet. Sci. Lett.*, 2001, no. 224, pp. 275–293.

38. Moyen, J-F., High Sr/Y and La/Yb Ratios: The Meaning of the "Adakitic Signature," *Lithos*, 2009, vol. 112, pp. 556–574.

39. Plechov, P.Yu. Opacitization Conditions of Hornblende in Bezymyannyi Volcano Andesites (March 30, 1956 Eruption), *Petrologiya*, 2007, vol. 15, no. 6, pp. 639–655 [*Petrology* (Engl. Transl.), 2008, vol. 16, no. 1, pp. 19–35].

40. Ponomareva, V.V., Kyle, P., Pevzner, M.M., et al., Holocene Eruptive History of Shiveluch Volcano, Kamchatka Peninsula, Russia, *Volcanism and Subduction: The Kamchatka Region*, Eichelberger J., Gordeev E., Izbekov P., Lees J. Eds., *AGU Geophys. Monogr.*, 2007, vol. 172, pp. 263–282.

41. Ponomareva, V.V., Pevzner, M.M., and Melekestsev, L.V., Large Debris, Avalanches, and Associated Eruptions in the Holocene Eruptive History of Shiveluch Volcano, Kamchatka, Russia, *Bull. Volcanol.,* 1998, no. 59, pp. 490–505.

42. Portnyagin, M.V. and Manea, V.C., Mantle Temperature Control on Composition of Arc Magmas Along the Central Kamchatka Depression, *Geology*, 2008, vol. 36, pp. 519–522.

43. Portnyagin, M.V., Bindeman, I.N., Hoernle, K., and Hauff, F., Geochemistry of Primitive Lavas of the Central Kamchatka Depression: Magma Genesis at the Edge of the Pacific Plate, in *Volcanism and Subduction: The Kamchatka Region*, Eichelberger J., Gordeev E., Izbekov P., and Lees J., Eds., *AGU Geophys. Monogr.*, 2007, vol. 173, pp. 203–244.

44. Richards, J.R. and Kerrich, R., Adakite-Like Rocks: Their Diverse Origins and Questionable Role in Metallogenesis, *Econ. Geol. Sp. Pap.*, 2007, vol. 102, no. 4, pp. 537–576.

45. Scaillet, B. and Evans, B.W., The 15 June 1991 Eruption of Mount Pinatubo. I. Phase Equilibria and Pre-Eruption $P–T–f_{O_2}–f_{H_2O}$ Conditions of the Dacite Magma, *J. Petrol.*, 1999, vol. 40, pp. 381–411.

46. Sparks, R.S.J., Sigurdsson, H., and Wilson, L., Magma Mixing Mechanism for Triggering Acid Explosive Eruptions, *Nature*, 1977, vol. 267, pp. 315–318.

47. Stern, C.R. and Kilian, R., Role of the Subducted Slab, Mantle Wedge and Continental Crust in the Generation of Adakites from the Andean Austral Volcanic Zone, *Contrib. Mineral. Petrol.*, 1996, vol. 123, pp. 263–281.

48. Streck, M.J., Leeman, W.P., and Chesley, J., High-Magnesian Andesite from Mount Shasta: A Product of Magma Mixing and Contamination, Not a Primitive Mantle Melt, *Geology*, 2007, vol. 35, pp. 351–354.

49. Tolstykh, M.L., Naumov, V.B., Babanskii, A.D., et al., Chemical Composition, Volatile Components, and Trace Elements in Andesitic Magmas of the Kurile–Kamchatka Region, *Petrologiya*, 2003, vol. 11, no. 5, pp. 451–470 [*Petrology* (Engl. Transl.), vol. 11, no. 5, pp. 407–425].

50. Trusov, S.V. and Plechov, P.Yu., Formation of Acid-to-Basic Series of Kizimen Volcano, Kamchatka, in *Mezhdunarodnoe petrograficheskoe soveshchanie "Petrografiya XXI veka"* (International Petrographic Conference "Petrography on the Turn of 21st Century"), Apatity, 2005, pp. 48–51.

51. Volynets, O.N., Geochemical Types, Petrology, and Genesis of Late Cenozoic Volcanic Rocks from the Kurile–Kamchatka Island Arc System, *Int. Geol. Rev.*, 1994, vol. 36, pp. 373–405.

52. Volynets, O.N., Heterotaxitic Lavas and Pumice, in *Problemy glubinnogo magmatizma* (Problems of Deep Magmatism), Moscow: Nauka, 1979, pp. 181–196.

53. Volynets, O.N., Ponomareva, V.V., and Babanskii, A.D., Magnesian Basalts of Shiveluch Andesite Volcano, Kamchatka, *Petrologiya*, 1997, vol. 5, no. 2, pp. 206–221 [*Petrology* (Engl. Transl.), vol. 5, no. 2, pp. 183–196].

54. Volynets, O.N., Ponomareva, V.V., Braitseva, O.A., et al., Holocene Eruptive History of Ksudach Volcanic Massif, South Kamchatka: Evolution of a Large Magmatic Chamber, *J. Volcanol. Geotherm. Res*, 1999, vol. 91, pp. 23–42.

55. Yogodzinski, G.M., Kay, R.W., Volynets, O.N., et al., Magnesian Andesite in the Western Aleutian Komandorsky Region: Implications for Slab Melting and Processes in the Mantle Wedge, *Geol. Soc. Am. Bull.,* 1995, vol. 107, no. 5, pp. 505–519.

56. Yogodzinski, G.M., Lees, J.M., Churikova, T.G., et al., Geochemical Evidence for the Melting of Subducting Oceanic Lithosphere at Plate Edges, *Nature*, 2001, vol. 409, pp. 500–504.

57. Zharinov, N.A. and Demyanchuk, Yu.V., Growth of Extrusive Dome of Shiveluch Volcano, Kamchatka, in 1980–2007 on the Basis of Geodetic Data and Video Filming, *Vulkanol. Seismol.*, 2008, no. 4, pp. 3–14.